

AD-A148 959

~~SECRET~~

(11)

SEMI-ANNUAL TECHNICAL REPORT

to the
AIR FORCE OFFICE OF SCIENTIFIC RESEARCH

from
Eugene Herrin

and
Tom Goforth

Dallas Geophysical Laboratory
Southern Methodist University
Dallas, Texas 75275

APPROVED FOR PUBLIC RELEASE
DISTRIBUTION IS UNLIMITED (A)

DARPA Order: 3291
Program Code: TF10
Name of Contractor: Southern Methodist University
Effective Date of Contract: July 15, 1976
Contract Expiration Date: September 30, 1979
Total Amount of Contract Dollars: \$407,466
Contract Number: F49620-76-C-0030
Principal Investigator and Phone Number: Eugene Herrin
AC 214 692-2760
Program Manager and Phone Number: Truman Cook, Director of
Research Administration
AC 214 692-2031
Title of Work: Propagation Path Effects for Rayleigh and
Love Waves
University Account Number: 80-88

DTIC FILE COPY

Sponsored by
Defense Advanced Research Projects Agency
DARPA Order No. 3291

DTIC
ELECTE
S
JAN 7 1985

84 12 27 112

→ A

SURFACE WAVE STUDIES
OF THE
BERING SEA AND ALASKA AREA

by
Doo Jung Jin

Accession For	
NTIS GRA&I	<input checked="" type="checkbox"/>
DTIC TAB	<input type="checkbox"/>
Unannounced	<input type="checkbox"/>
Justification	
By	
Distribution/	
Availability Codes	
Dist	Avail and/or Special
A1	



Geophysical Laboratory
Southern Methodist University
Dallas, Texas 75275
31 January 1979

ABSTRACT

The area of the Bering Sea and Alaska has been studied in terms of shear-velocity, density and compressional-velocity structure by applying a generalized linear inversion method to fundamental-mode Rayleigh-wave group-velocity dispersion relationships in the period range from 10 to 100 sec.

Group velocity dispersion relationships in the area have been obtained by applying the phase-matched filtering technique (Herrin and Goforth, 1977) to digitally recorded surface-wave data. Corrections for instrument response and the sphericity of the Earth were applied to the dispersion observations. A new exact analytical method for the computation of Rayleigh-wave phase-velocity partial derivatives with respect to Earth parameters has been formulated. With the phase-velocity partial derivatives determined, the group velocity partial derivatives were computed by use of the fast and accurate method of Rodi, et al. (1975), and were successfully incorporated into a generalized linear inversion method.

The study area has been found to consist of three physiographic provinces and the structure of the three regions has been estimated as follows: In continental Alaska, the crustal thickness is 43 ± 3 km, and a low velocity zone extends from a depth of about 113 km to about 213 km. In the Bering Shelf region, the depth to the Mohorovicic discontinuity is 28 ± 4 km, and a low velocity zone ranges in depth from about 108 km to about 213 km. In the Aleutian Basin, the thickness of the crust is 18 ± 4 km, and a low velocity zone extends from a depth of about 60 km to about 220 km.

TABLE OF CONTENTS

	<u>Page</u>
ABSTRACT	iv
TABLE OF CONTENTS.	vi
LIST OF TABLES	viii
LIST OF ILLUSTRATIONS.	ix
ACKNOWLEDGMENTS.	xi
INTRODUCTION	1
DATA	5
METHOD	16
Phase-matched Filtering.	16
Division of the Study Area into Different Provinces	17
Corrections to the Observed Data	19
Uncertainty in the Observed Data	22
Method for the Computation of Partial Derivatives	23
Generalized Linear Inversion	28
Propagation of Errors.	36
Consideration for Model Parameters with Different Dimensions	37
RESULTS AND DISCUSSION	40
Continental Alaska	44
Bering Shelf	56
Aleutian Basin	64

CONCLUSION	81
APPENDIX	83
BIBLIOGRAPHY	89

LIST OF TABLES

<u>Table</u>	<u>Title</u>	<u>Page</u>
1	Earthquakes Used in the Study	10
2	Proportion of Path Lengths in Different Provinces	20
3	Instrument Corrections.	41
4	Sphericity Corrections.	41
5	Initial Model for the Structure of Continental Alaska.	45
6	Initial Model for the Structure of the Bering Shelf.	58
7	Initial Model for the Structure of the Aleutian Basin.	68

LIST OF ILLUSTRATIONS

<u>Figure</u>	<u>Title</u>	<u>Page</u>
1	Map of the Study Area with Locations of the Seismographic Station (ALPA) and Epicenters of the Seismic Events Studied Shown. Mercater Projection.	6
2	Instrument Amplitude Response.	7
3	Instrument Phase Response.	8
4a,b,c d,e	Seismograms of the Events Used	11-15
5	Observed Group Velocity Dispersion for the Events Used.	43
6	Group Velocity Partial Derivatives with Respect to Shear Velocity in Alaska.	46
7	Group Velocity Partial Derivatives with Respect to Density in Alaska	47
8	Group Velocity Partial Derivatives with Respect to Compressional Velocity in Alaska	48
9	Structure of the Final Model for Continental Alaska	49
10	Observed and Predicted Group Velocities for Continental Alaska	51
11	Resolving Kernels for Shear Velocity in Continental Alaska	54
12	Resolving Kernels for Density in Continental Alaska	55
13	Information Density in Continental Alaska. . .	57
14	Group Velocity Partial Derivatives for T=25 in the Bering Shelf.	59

15	Group Velocity Partial Derivatives for T=40 in the Bering Shelf	60
16	Structure of the Final Model for the Bering Shelf	62
17	Observed and Predicted Group Velocities for the Bering Shelf	63
18	Resolving Kernels for Shear Velocity in the Bering Shelf	65
19	Resolving Kernels for Density in the Bering Shelf	66
20	Information Density in the Bering Shelf.	67
21	Group Velocity Partial Derivatives for T=16 in the Aleutian Basin.	69
22	Group Velocity Partial Derivatives for T=50 in the Aleutian Basin.	70
23	Structure of the Final Model for the Aleutian Basin	71
24	Observed and Predicted Group Velocities for the Aleutian Basin	73
25	Resolving Kernels for Shear Velocity in the Aleutian Basin	75
26	Resolving Kernels for Density in the Aleutian Basin	76
27	Information Density in the Aleutian Basin.	77
28	Observed and Predicted Group Velocities for Event 1519	79
29	Observed and Predicted Group Velocities for Event 2005	80

ACKNOWLEDGMENTS

In the course of my degree program at Southern Methodist University, I have been deeply indebted to many people. I would like to gratefully acknowledge them on this occasion of the completion of my thesis.

Many thanks, for which I cannot possibly find a proper expression, are due to my thesis advisor, Professor Eugene Herrin, who has been teaching, stimulating, guiding and helping me with his convincing theory, skillful practicality and financial assistance, in my whole educational process at S.M.U. in general and in my thesis research, from the conception to delivery of this thesis, in particular. Professor Wayne Peeples has provided invaluable assistance through his teaching and insightful discussions in the course of my study, especially in connection with the generalized linear inversion part of my thesis research, which was not possible without his help. Many thanks also go to Dr. Thomas Goforth, Assistant Director of the Geophysical Laboratory, who has generously shared his time with me in many stimulating discussions and has provided practical guidance. I wish to thank Professor Thomas Williams, Professor Jeff D. Chalk of the Physics Department, and Dr. Harry Mack of Mobil Research and Development Corporation, who have encouraged and assisted me in many ways and convened at inconvenient times to steer my research.

Nancy Cunningham, Director of I.S.E.M. Computer Center, and Janet Taylor, Manager of User Services, Bradfield Computation Center, have been most helpful and always willing to render their assistance in effective use of computer resources, data processing and problem shooting. Mrs. Mattie Sue Mounce, Librarian of the Science Information Center, has provided most effective and efficient assistance in dealing with printed information. Liebe Purnell, with her constant smile, has been a most kind and efficient administrative helper.

I also wish to thank those who have provided me with financial assistance, which was vital to my research. This work was supported, in part, by Professor Eugene Herrin's research funds provided by the Defense Research Projects Agency under Contract F49620-76-C-0030, monitored by the Air Force Office of Scientific Research and by National Science Foundation Grant EAR-77-13714; by Institute for the Study of Earth and Man Projects 20-91-235-020 and 20-91-236-044; and by funds from Southern Methodist University, for which Professor Michael Holdaway, chairman of the department, has been most helpful and considerate.

Lastly, I am grateful to my family--my wife and three children--who have helped me to perform a dual role of a family member and graduate student for the long years of my graduate studentship, and to many friends who have constantly been concerned about my progress and encouraged me.

INTRODUCTION

Seismic surface waves have drawn much of seismologists' attention in the last few decades, partly due to their ability to sample the outer part of the earth over long paths and to provide information on average structures for parts of the earth which are not readily accessible to body wave studies; and partly due to their usefulness in discrimination between natural and artificial seismic sources, and in estimation of the source parameters.

The objective of this study is to further our understanding of the structure of the earth by investigating the crustal and uppermost mantle structure of the Bering Sea and of Alaska. In order to accomplish this goal, group velocity relationships have been determined by applying the phase-matched filtering technique (Herrin and Goforth 1977) to observed surface wave data. In the course of inverting the group velocity dispersion relationships, in order to obtain the shear-wave velocity, density and compressional-wave velocity structure of the area, a new method for the computation of Rayleigh-wave phase-velocity partial derivatives with respect to earth parameters was formulated. With the phase-velocity partial derivatives determined, the fast and accurate method of Rodi et al. (1975) was used for computing

the group-velocity partial derivatives. In conjunction with this new method, a generalized linear inversion technique was used for the inversion of the group velocity dispersion relationships.

The area of the Bering Sea and Alaska was chosen to be investigated for the following reasons: (i) This area bears geophysical and tectonic importance in that it is located along the plate boundary between the Pacific and North American plates and is adjacent to the boundary between the North American and Eurasian plates. (ii) This area is a region of primary significance for seismic surveillance from the United States' point of view (Evernden, 1969). (iii) This area may be unusual in that the crust of the Aleutian Basin region may be undergoing the process of the continentalization of an oceanic crust (Shor, 1964). (iv) Finally, this area has not, to this author's knowledge, been studied before in detail and on a regional basis.

It was decided to work on group velocities rather than phase velocities with the following reasons: (i) As mentioned above, the phase-matched filtering technique, which is an accurate method for determining group-velocity dispersion, was readily available. (ii) It is well known that group and phase velocity observations provide basically the same information about the earth model (Der, et al., 1970; Wiggins, 1972). Pilant and Knopoff (1970) have shown that inversion of phase velocities eliminates one degree of

non-uniqueness compared with inversion of group velocities since group velocities are a derivative property of phase velocities. However, as pointed out by Yu and Mitchell (1979), due to the very nature of the group velocity as a differential of the phase velocity, small perturbations in phase velocity show up as larger variations in group velocity. Thus the group velocity dispersion, when inverted, should produce a more detailed earth model. Braile and Keller (1975) have stated that the inversion of group velocities did not appear to have degraded the results in comparison with those from the inversion of phase velocities. (iii) The aperture of the Alaskan Long Period Array (ALPA) used as the recording station may be too small to yield reliable phase velocity information.

Preliminary inspection of data showed that the quality of Love-wave data was inferior to that of Rayleigh-wave data. It was also found that Love-wave dispersion contributes less information about earth structure than Rayleigh-wave dispersion (Der et al., 1970; Braile and Keller, 1975). Since, in general, the maxima of the Rayleigh-wave partial-derivative curves are larger and narrower than those of the corresponding Love-wave curves, Rayleigh waves give better resolution than Love waves. For the above reasons, it was decided to use only Rayleigh waves in this study.

Inspection of results of the multiple filter analysis (Dziewonski et al., 1969), showed that there was not much

energy present in higher modes. Under this circumstance, efforts to use higher modes may introduce erroneous rather than useful information. Therefore it was decided to work with only fundamental-mode Rayleigh waves.

DATA

The data used in this study were collected at the Alaskan Long Period Array (ALPA). ALPA was selected as a recording station for the following reasons: (i) This seismic array, which is located just north of Fairbanks, Alaska, was probably the best, reliably equipped set of seismographic stations around the study area and data from it are suitable for accomplishing the objective of this research in that the array is located at one end of the region of interest, while the locations of the seismic sources range from near the array to the Komandorsky Islands. (ii) The quality of the data recorded at this array is known to be good. It is an array with an aperture of about 80 km and was installed with the knowledge and experience gained from the operation of the large aperture seismic array near Billings, Montana (LASA). (iii) Since the data is digitally recorded on magnetic tape, there is no possibility of error incurred from the digitization of analog data. (iv) Finally, the data were available for use in this research.

The location of the recording stations and the epicenters of the earthquakes used in this study are shown in Fig. 1. The relative amplitude and phase responses of the seismograph system are shown in Figs. 2 and 3, respectively. The parameters

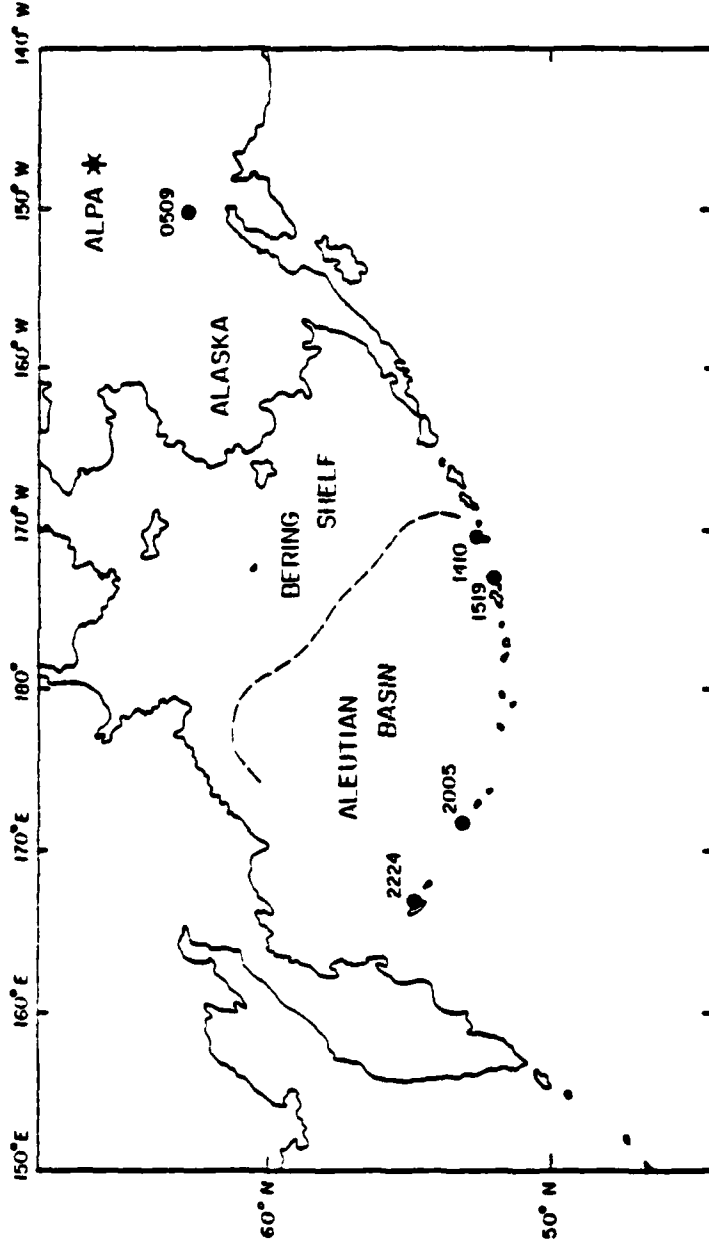


Figure 1: Map of the Study Area with Locations of the Seismographic Station (ALPA) and Epicenters of the Seismic Events Studied Shown. Mercator Projection

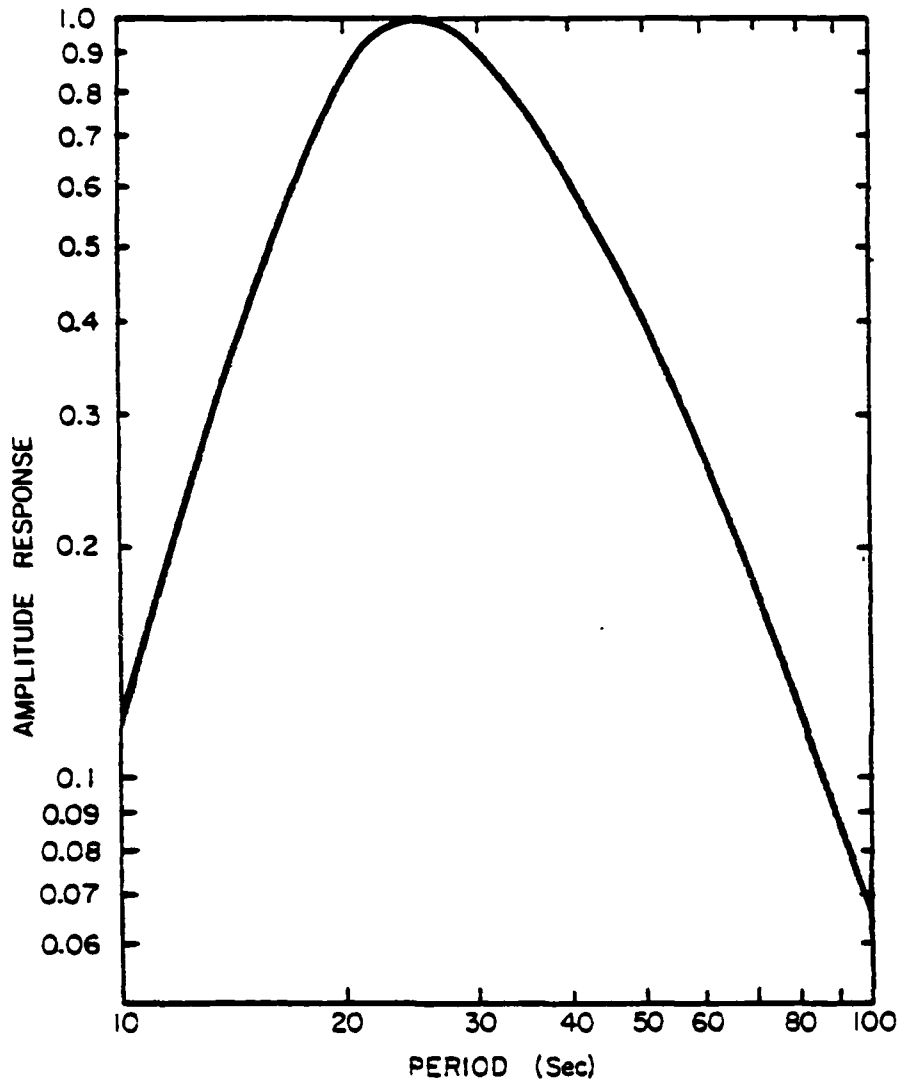


Figure 2: Instrument Amplitude Response

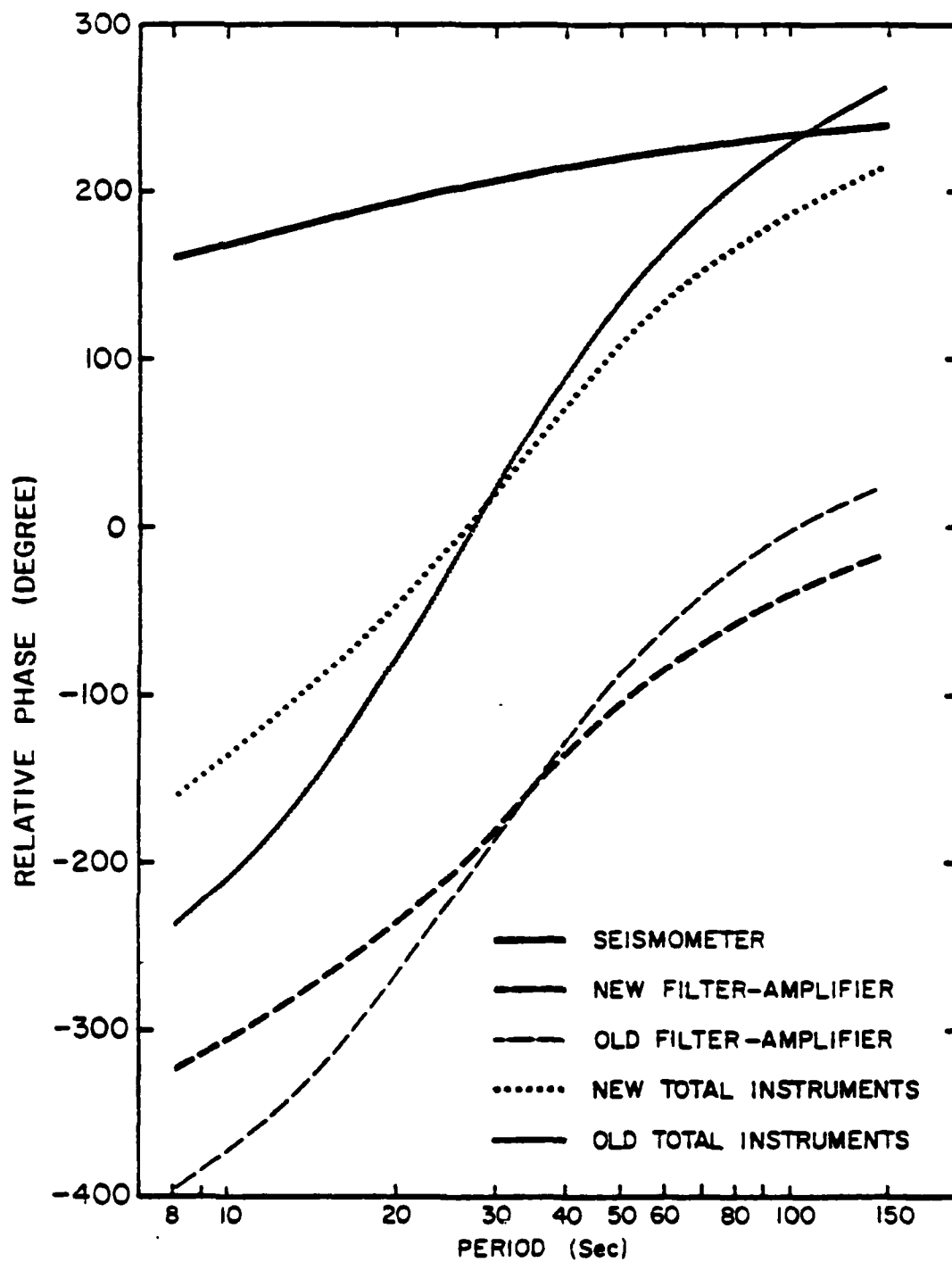


Figure 3: Instrument Phase Response

of the earthquakes used are listed in Table 1. The information on source parameters is from the Preliminary Determination of Epicenters (PDE) published by either the National Oceanic and Atmospheric Administration or the United States Geological Survey National Earthquake Information Service. The vertical-component seismograms of the events studied are shown in Figs. 4a to 4e.

TABLE 1
EARTHQUAKES USED IN THE STUDY

Event Name	Origin Time (Y-Mo-D-H-MI-S)	Latitude (deg)	Longitude (deg)	Depth (km)	m_b	Distance (km)
0509	1972-04-11-18-21-35.5	62.0N	150.4W	18	4.5	421.81
1410	1972-08-26-11-38-09.8	52.5N	170.6W	52	4.7	1916.86
1519	1974-07-20-00-48-03.9	51.6N	173.5W	45	4.9	2121.57
2005	1971-12-14-02-29-26.7	52.8N	172.0E	38	4.9	2600.91
2224	1975-11-04-12-05-56.9	54.4N	167.5E	24	5.5	2756.70

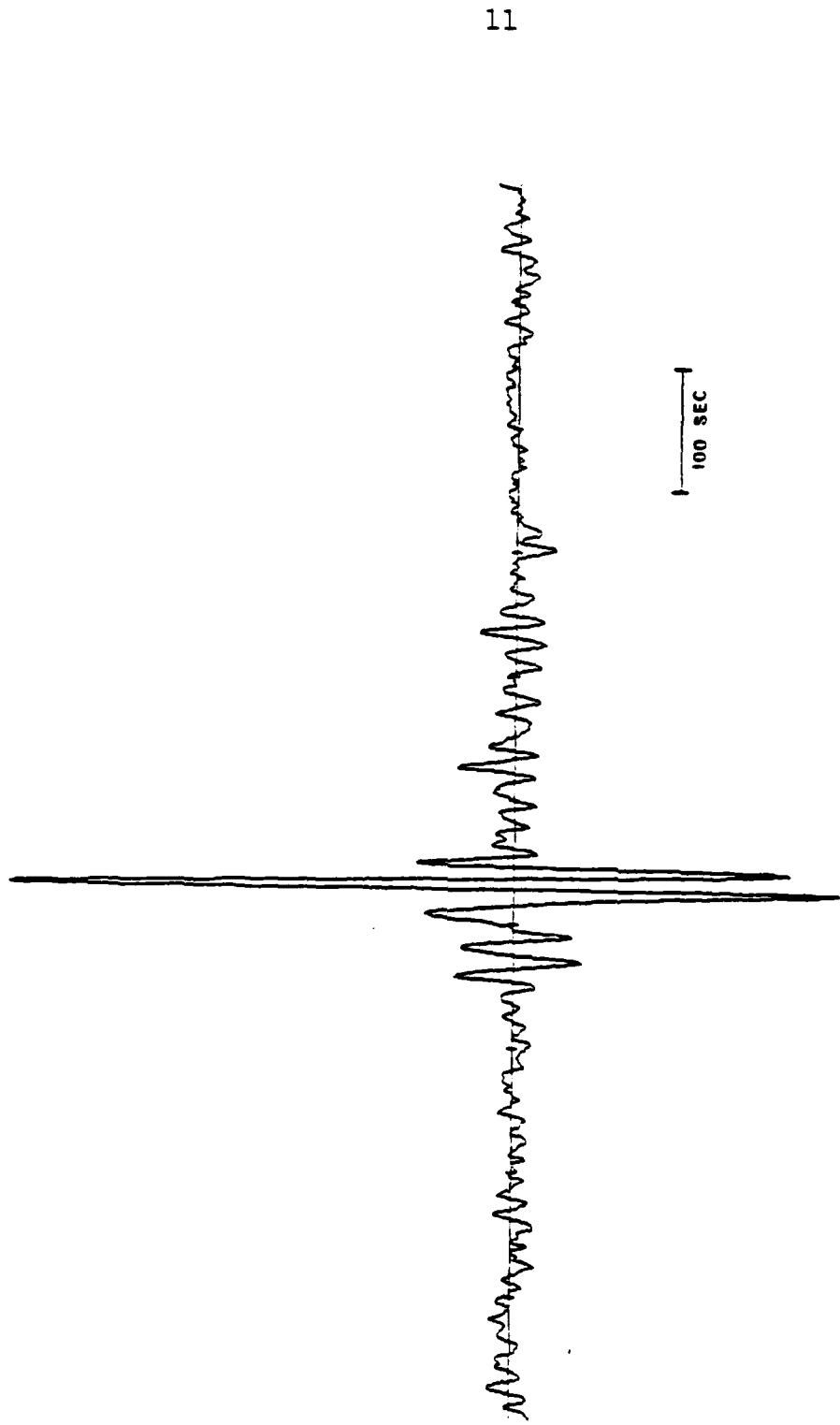


Figure 4a: Vertical-component Seismogram of Event 0509

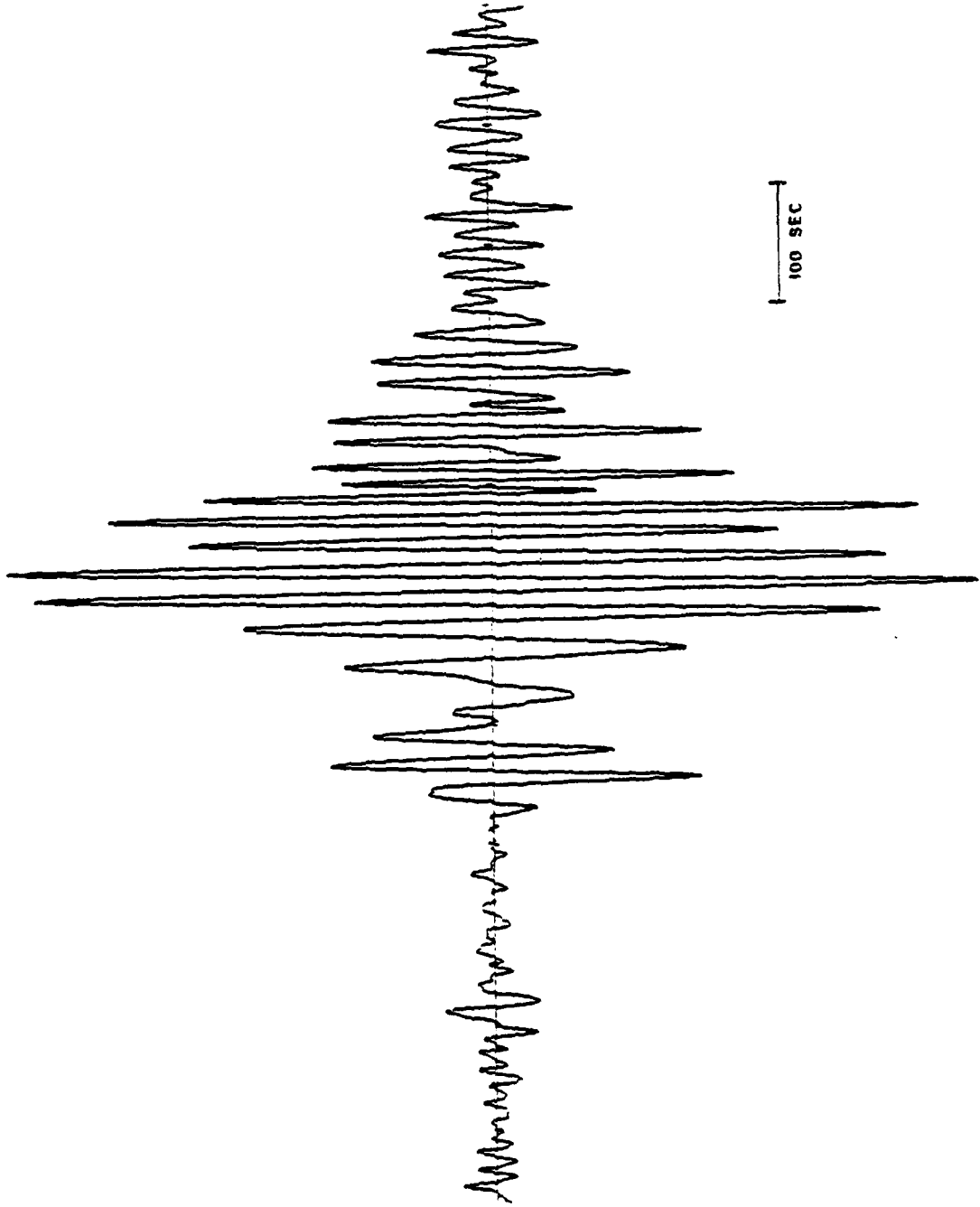


Figure 4b: Vertical-component Seismogram of Event 1410

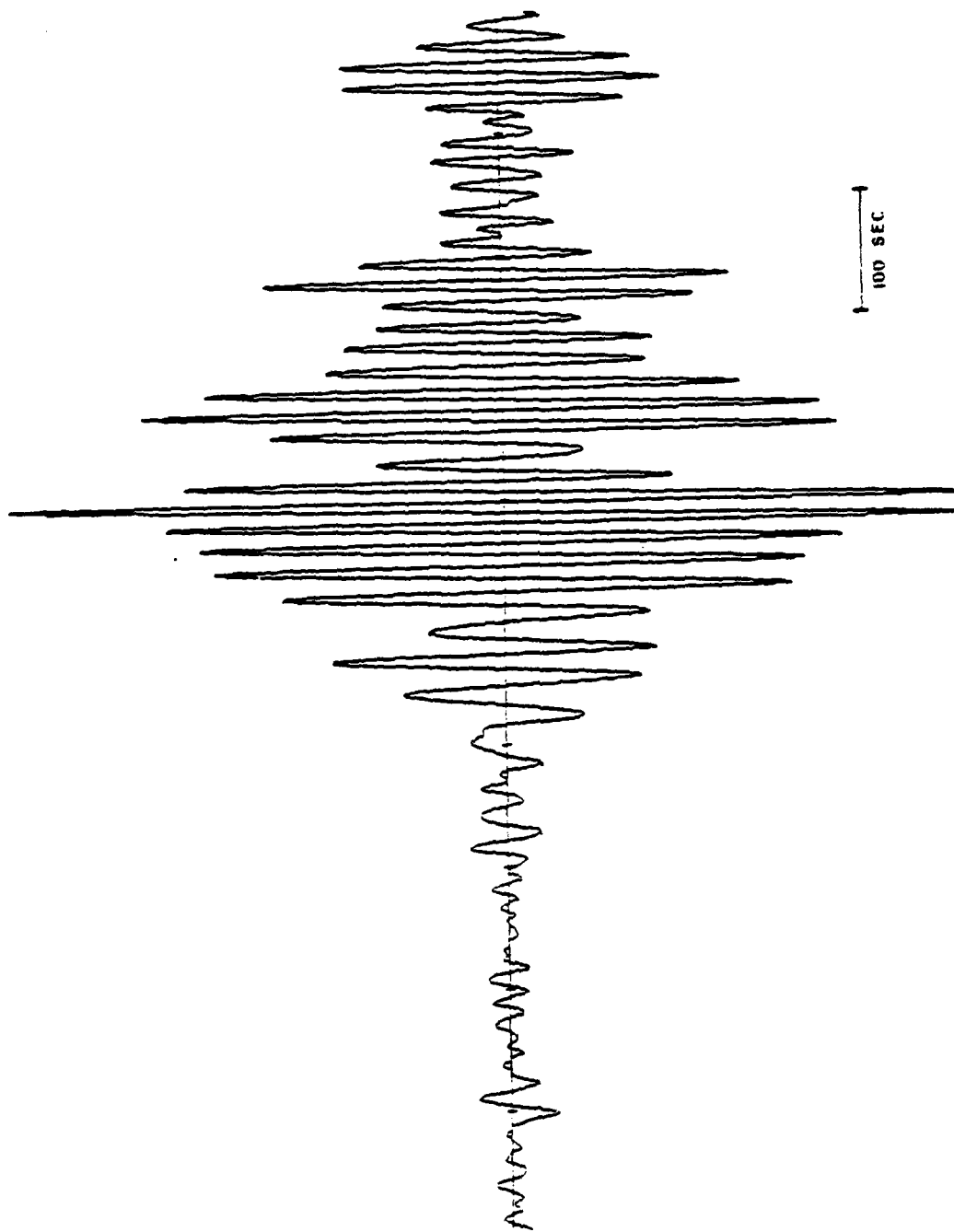


Figure 4c: Vertical-component Seismogram of Event 1519

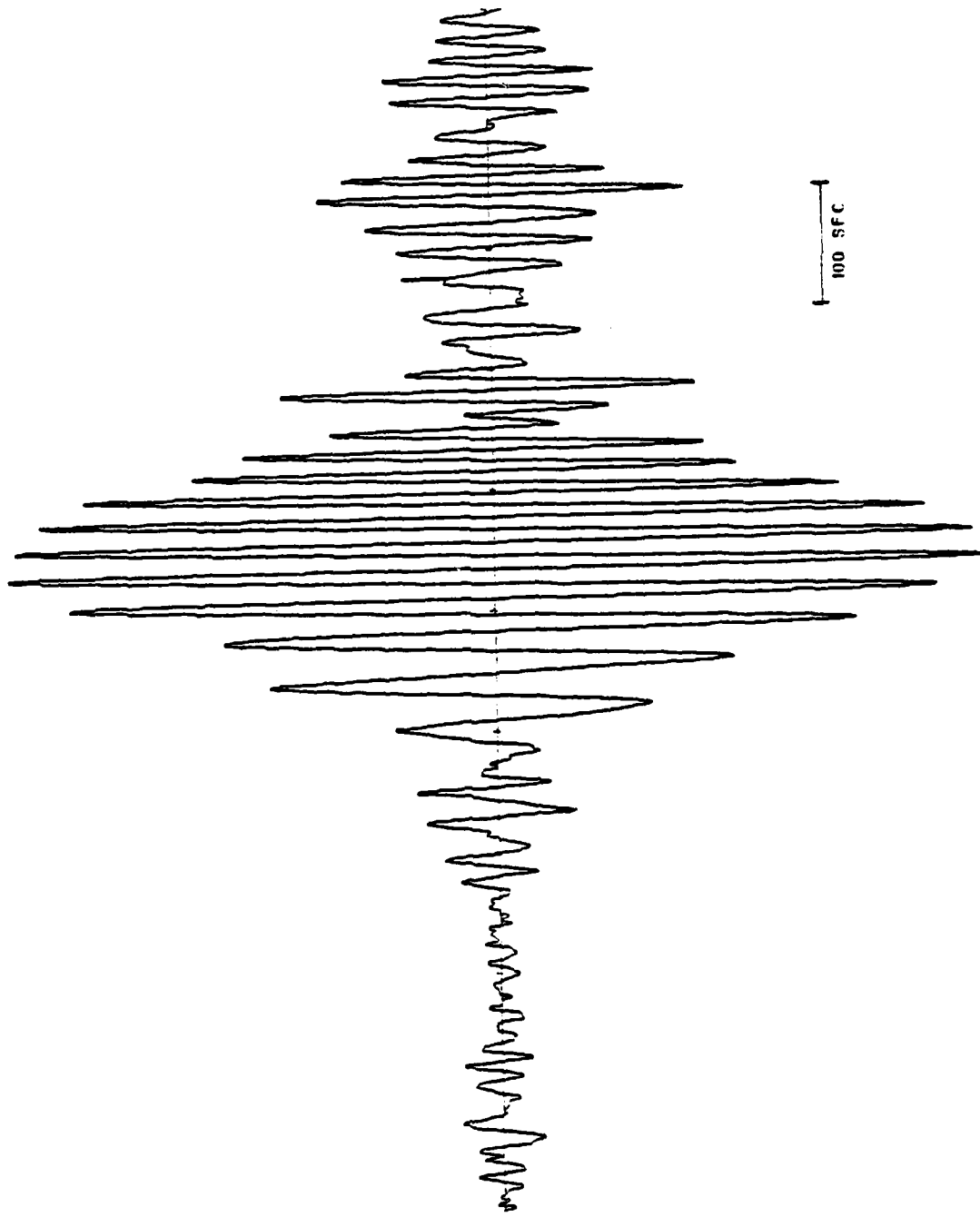


Figure 4d: Vertical-component Seismogram of Event 2005

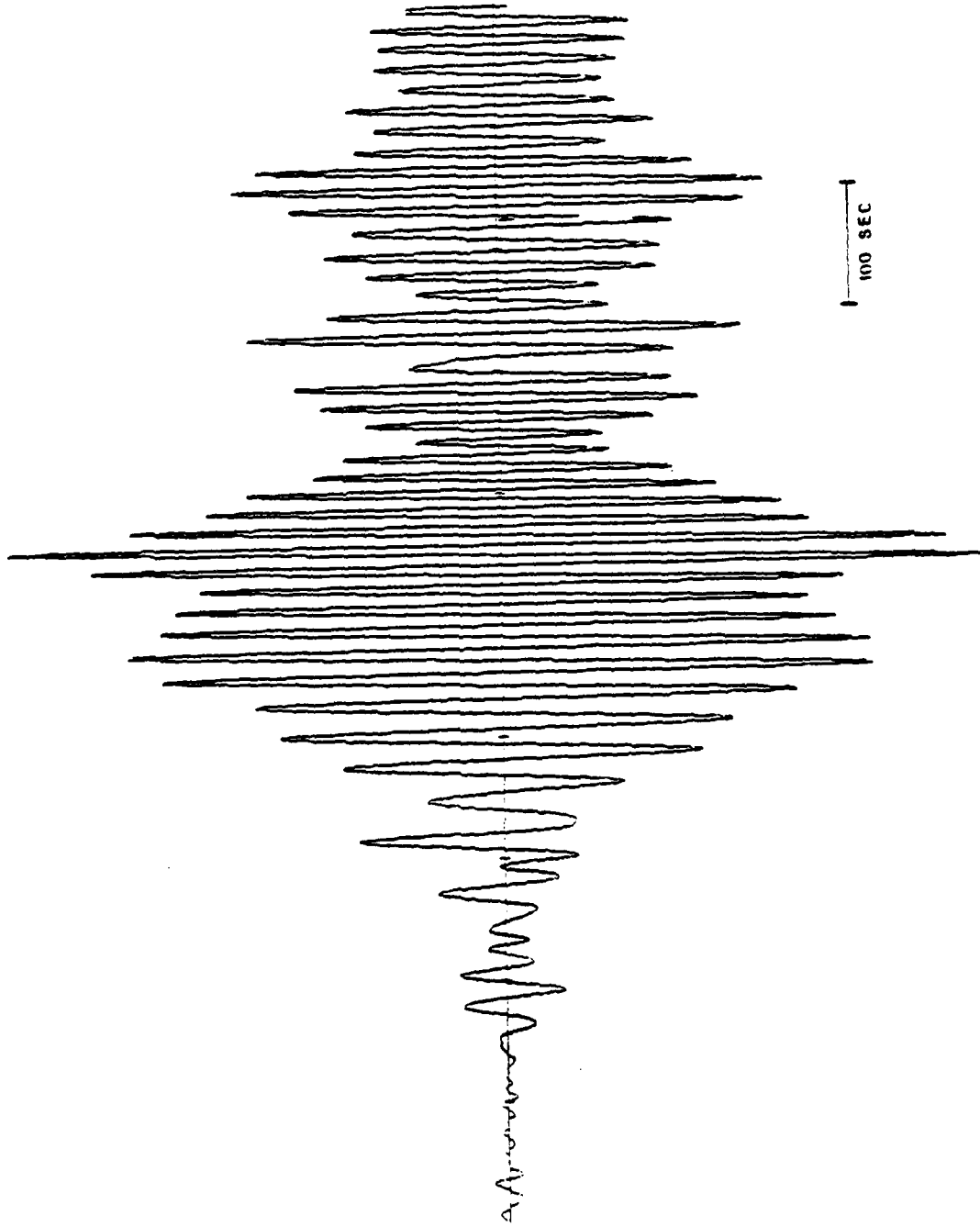


Figure 4e: Vertical-component Seismogram of Event 2224

METHOD

1. Phase-matched Filtering

For the determination of the dispersion relationships of surface waves, Dziewonski et al. (1969) have developed a method called multiple filter analysis. Realizing the lack of resolution in the time domain of the above method, a more capable method called phase-matched filtering has been developed and proved effective in more recent studies by Herrin and Goforth (1977). The phase-matched filtering technique was used in this study in order to separate the effects of the multipathing from those of primary arrivals. In using the phase-matched filter, a dispersion curve obtained from the multiple filter analysis was used as the initial input to the iterative procedure of the phase-matched filtering technique.

Since the original papers give full accounts of the above methods, only a brief description of the methods is given below. The multiple filter analysis technique displays, as its product, the instantaneous amplitude of a seismogram as a function of both period and group velocity (time). When the instantaneous amplitudes are contoured, a line connecting the maximum amplitudes for specified periods, which is represented by the ridge crest of the contour diagram, gives the group velocity dispersion relationships for the analyzed seismogram.

In the phase-matched filtering technique, the Fourier phase of the filter is made equal to that of a given seismogram with the possibly existing multipath effects removed. The group delays for the initial input dispersion curve are computed. The phase of the filter is calculated by integrating the above-obtained group delays. By crosscorrelating the filter and the given seismogram and windowing the cross-correlation function, the phase of the filter is made equal to that of the seismogram after a certain number of iterations. The group delays of the filter are corrected as the phase of the filter is modified in each iteration. The group velocity is then computed from the final group delays of the phase-matched filter.

2. Division of the Study Area into Different Provinces

The study area was divided into three physiographic provinces--continental Alaska, the Bering Shelf, and the Aleutian Basin. This classification was chiefly based on topographic and bathymetric data of the area and is shown in Fig. 1. The boundary between the Bering Shelf and the Aleutian Basin was drawn along the 1000-fathom contour line of bathymetric data. One purpose of this study was to study the structure of the three provinces and to determine the boundary between them if they are different in structure.

Although it appeared from the topographic and bathymetric data that continental Alaska and the Bering Shelf are

continental and the Aleutian Basin is oceanic in crustal and uppermost mantle structure, there was, as pointed out in the introduction, a possibility of the Aleutian Basin's being continental in nature. As an attempt to resolve this problem, the following method was used.

By inverting the group velocity dispersion relationship obtained from the event 0509, whose epicenter is located within continental Alaska, a structure for continental Alaska was determined. It was recognized that the great circle path for the event 1410, which is located near the western edge of the Bering Shelf, crosses the boundary between continental Alaska and the Bering Shelf at a nearly right angle. The proportion of the lengths of continent and shelf along the great circle path was measured on a globe. By subtracting the group velocity dispersion proportional to the continental path from the observed group velocity dispersion for the event 1410, the observed group velocity dispersion relationship for the pure shelf path was derived. By inverting the resultant group velocity dispersion, the structure of the shelf region was determined.

Similarly, it was found that the great circle path for the event 2224, which is located near the western end of the Aleutian Basin, crosses the boundary between continental Alaska and the Bering Shelf and the boundary between the latter and the Aleutian Basin, both nearly perpendicularly. The group velocity dispersion relationships determined above for continental Alaska and the Bering Shelf were subtracted in proportion to their segment lengths of the great circle path

from the observed group velocity dispersion of event 2224 to derive the observed group velocity dispersion relationship for the pure Aleutian Basin path.

Before committing much effort to find the detailed structure of the study area, reasonableness of the above line of thinking was tested by applying the above procedure with average earth models of Dziewonski et al. (1975) to the observed data corrected for instrument response. The results were encouraging, and the above division of the study area was adopted for subsequent studies. The proportion of lengths of different provinces along the great circle path for the events used in this study is shown in Table 2.

3. Corrections to the Observed Data

Two types of corrections were applied to the group velocity dispersion relationships determined from the phase-matched filtering technique. One is for the instrument phase responses and the other is for the sphericity and gravity of the earth.

For the instrument correction, the following relationship was used:

$$t_g(\omega) = \frac{d\phi(\omega)}{d\omega} \quad (1)$$

where $t_g(\omega)$ and $\phi(\omega)$ are, respectively, the group delay and phase response of the instruments for an angular frequency ω . The phase responses of the instruments as shown in Fig. 3 were used for this purpose.

TABLE 2
PROPORTION OF PATH LENGTHS IN DIFFERENT PROVINCES

<u>Event Name</u>	Proportion of Distances		
	<u>Continental</u>	<u>Shelf</u>	<u>Oceanic</u>
1410	0.50	0.50	0.00
1519	0.51	0.30	0.19
2005	0.39	0.27	0.34
2224	0.25	0.40	0.35

During the summer of 1972, the seismograph filter-amplifiers were replaced with new units having different characteristics. Two different response curves for the corresponding filter-amplifier systems are shown in Fig. 3. Events 0509 and 2005 were recorded with the old instruments while the rest of the events were recorded with the new instruments.

The observed group velocities as obtained from the phase-matched filtering technique represent the dispersion of the gravitating spherical earth, while the calculation of the group velocities in the process of inversion is, for computational convenience, made for a nongravitating plane-layered earth model. Therefore it is necessary to convert the observed group velocity dispersion to one corresponding to the nongravitating plane-layered earth.

For Love waves it is possible to apply a suitable transformation to the plane-layered earth model to simulate the effects of sphericity (Gerver and Kazhdan, 1968; Biswas and Knopoff, 1970). For Rayleigh waves, however, a similar transformation is difficult to achieve and an empirical correction must be applied. Such a correction has been derived by Bolt and Dorman (1961) and has been widely used. After fifteen years, North and Dziewonski (1976), based on studies with additional and presumably better earth models, have improved the formula of Bolt and Dorman (1961).

Since the effects of sphericity and gravity upon group velocity are much less than those upon phase velocity, as

pointed out by Bolt and Dorman (1961) and North and Dziewonski (1976), a quarter of the difference between the phase velocities of gravitating spherical earth and nongravitating plane-layered earth, as shown in Table 1 of North and Dziewonski (1976) was used in the present study as a somewhat arbitrary but reasonable difference between the group velocities of the above two representations of the earth (see Figs. 4 to 6 of Bolt and Dorman, 1961). For the regions of continental Alaska, the Bering Shelf and the Aleutian Basin, the velocity differences of the earth models ANDES, PLATFORM and PEMOCD, respectively, of North and Dziewonski (1976) were used. Since it was found that the velocity differences of North and Dziewonski are smoothly varying quantities with period, their values were interpolated or extrapolated as necessary in the present study.

4. Uncertainty in the Observed Data

Der et al. (1970) used the uncertainty principle of Bendat (1958) in assessing the uncertainties in their group velocity data obtained by the multiple filter analysis technique. Judging that the multiple filter analysis gives an accuracy greater than that from the uncertainty principle, they took one-fifth of the error estimated from the uncertainty principle as their error of measurements. They gave 0.01 km/sec as a lower error limit; 0.03 km/sec was adopted as the uncertainty of the group-velocity data by Braile and Keller (1975) without an explicit explanation, and by Yu and Mitchell (1979) who used the multiple filter analysis method.

Although, in the present study, the phase-matched filtering, which is considered to be much more accurate than the multiple filter analysis, is used, 0.03 km/sec was taken as the maximum error in the group-velocity data. This value is adopted in order to accommodate the possible errors in applying the instrument and sphericity-gravity corrections.

5. Method for the Computation of Rayleigh-wave Phase-velocity Partial Derivatives with Respect to Earth Parameters

In the inversion of group velocity dispersion observations it is necessary to compute the partial derivatives of group velocities with respect to various earth parameters. Since a fast and accurate method has been developed for computing group velocity partial derivatives when corresponding phase velocity partial derivatives are known (Rodi et al., 1975), an effort was made in the present study to formulate a simple new method for the computation of exact phase-velocity partial derivatives. The following paragraphs are the outcome of this effort.

In an earth model in which the earth consists of many elastic, homogeneous and isotropic parallel layers on a homogeneous and isotropic half-space, the earth properties may be defined by longitudinal and transverse wave velocities, density, and thickness of the component layers. Various methods have been employed in computing the phase-velocity partial derivatives with respect to the above model parameters.

Dorman and Ewing (1962), followed by Brune and Dorman (1963), calculated the changes in phase velocity due to the

perturbation of each physical parameter while retaining the remaining parameters constant. This method is very time-consuming. On the basis of Jeffreys' (1961) suggestion that Rayleigh's principle can be used to find expressions for the effects of small changes of the elastic properties on the phase velocity, Anderson (1964) and Takeuchi et al. (1964), followed by Harkrider (1968) and Anderson and Harkrider (1968), approached the problem by using the energy integral technique. This technique is quite complex. McEvelly (1964) has used a combination of the above two methods. Bloch et al. (1969), Der et al. (1970), Der and Landisman (1972) and Knopoff (1972) have computed phase-velocity partial derivatives but they have not described the algorithm they employed. Novotny (1970) derived exact expressions for Love-wave phase velocity partials in a different way by taking advantage of Thomson-Haskell matrices (Thomson, 1950; Haskell, 1953).

In the rest of this section, following Novotny in Love waves, a new method of computing the Rayleigh-wave phase-velocity partial derivatives with respect to the parameters of the medium is presented. Convenient formulas for the Haskell layer-matrix derivatives, which are necessary in the computation of the phase-velocity partial derivatives, are given in the Appendix. Employing double precision in computer programming, the use of the Haskell layer-matrix method has not shown any numerical difficulties (Thrower, 1965; Dunkin, 1965; Gilbert and Backus, 1966, among others) in the period range of 10 to 100 sec, as used in this study.

Harkrider (1964) has derived a matrix equation for the dispersion of Rayleigh waves, which may be expressed as follows:

$$F(c, \omega, \alpha_m, \beta_m, \rho_m, d_m) = NK + L^*M^* - T^*(G^*N - L^*H) \quad (2)$$

where

$$c = c(\omega, \alpha_m, \beta_m, \rho_m, d_m),$$

$$T^* = c^2 \rho_0 \tan P_0 / \rho_{\alpha 0}$$

and

$$\begin{aligned} L &= \gamma_n \rho_{\alpha n} A_{11} + (\gamma_n - 1) A_{21} - (\rho_{\alpha n} A_{31} - A_{41}) / (c^2 \rho_n) \\ K &= \gamma_n \rho_{\alpha n} A_{12} + (\gamma_n - 1) A_{22} - (\rho_{\alpha n} A_{32} - A_{42}) / (c^2 \rho_n) \\ G &= \gamma_n \rho_{\alpha n} A_{13} + (\gamma_n - 1) A_{23} - (\rho_{\alpha n} A_{33} - A_{43}) / (c^2 \rho_n) \\ N &= -(\gamma_n - 1) A_{11} + \gamma_n \rho_{\beta n} A_{21} + (A_{31} + \rho_{\beta n} A_{41}) / (c^2 \rho_n) \\ M &= -(\gamma_n - 1) A_{12} + \gamma_n \rho_{\beta n} A_{22} + (A_{32} + \rho_{\beta n} A_{42}) / (c^2 \rho_n) \\ H &= -(\gamma_n - 1) A_{13} + \gamma_n \rho_{\beta n} A_{23} + (A_{33} + \rho_{\beta n} A_{43}) / (c^2 \rho_n) \end{aligned} \quad (3)$$

Here ω is the angular frequency, c phase velocity, α and β velocities of compressional and shear waves, ρ density, d thickness of a layer;

$$\gamma_m = 2(\beta_m/c)^2,$$

$$P_m = k d_m \rho_{\alpha m}, \quad Q_m = k d_m \rho_{\beta m}$$

where k represents the wave number;

$$\mathcal{L}_{\alpha m} = \begin{cases} (c^2/\alpha_m^2 - 1)^{1/2}, & c > \alpha_m \\ -i(1 - c^2/\alpha_m^2)^{1/2}, & c < \alpha_m \end{cases};$$

$$\mathcal{L}_{\beta m} = \begin{cases} (c^2/\beta_m^2 - 1)^{1/2}, & c > \beta_m \\ -i(1 - c^2/\beta_m^2)^{1/2}, & c < \beta_m \end{cases}$$

where $i = (-1)^{1/2}$;

$$A = a_{n-1} a_{n-2} \cdots a_1$$

with a_m designating the Haskell's layer matrix for the m th layer; and subscripts m , n and o refer to the m th solid layer, half-space and liquid surface layer, respectively. In order to minimize typographical requirements, a compound subscript, e.g. α_m , is used where a subscripted subscript is appropriate. An asterisk superscript is used to transform an imaginary quantity into a real one such that $Z^* = Z/i$ for an arbitrary imaginary quantity Z .

Since $T^* = 0$ for the earth model in which the liquid surface layer does not exist, considering (2) is sufficient for earth models both with and without ocean. From (2),

$$\frac{\partial c}{\partial x} = - \frac{\partial F}{\partial x} / \frac{\partial F}{\partial c} \quad (4)$$

where x designates one of the earth parameters α , β , ρ and d .

If we define two product matrices A_m and B_m such that

$$A_m = a_m a_{m-1} \cdots a_1 \quad (5)$$

$$B_m = a_{n-1} a_{n-2} \cdots a_m$$

then

$$A = B_{m+1} \cdot a_m \cdot A_{n-1}$$

$$\frac{\partial A_{ij}}{\partial X_m} = \left[B_{m+1} \cdot \frac{\partial a_m}{\partial X_m} \cdot A_{m-1} \right]_{ij}, \quad m = 2, 3, \dots, n-2 \quad (6)$$

$$\frac{\partial A_{ij}}{\partial c} = \left[\frac{\partial a_{n-1}}{\partial c} A_{n-2} + \sum_{m=2}^{n-2} B_{m+1} \cdot \frac{\partial a_m}{\partial c} \cdot A_{m-1} + B_2 \frac{\partial a_1}{\partial c} \right]_{ij}$$

For the particular cases where $m=1$ and $m=n-1$, respectively, the second equation of (6) becomes

$$\frac{\partial A_{ij}}{\partial X_1} = \left[B_2 \cdot \frac{\partial a_1}{\partial X_1} \right]_{ij}$$

and

$$\frac{\partial A_{ij}}{\partial X_{n-1}} = \left[\frac{\partial a_{n-1}}{\partial X_{n-1}} \cdot A_{n-2} \right]_{ij}.$$

It is noted from (2) and (3) that in order to compute $\frac{\partial F}{\partial X_m}$ we need $\frac{\partial A_{ij}}{\partial X_m}$, and that in order to compute $\frac{\partial F}{\partial c}$ we need

$$\frac{\partial A_{ij}}{\partial c}, \quad \frac{\partial T^*}{\partial c}, \quad \frac{\partial \lambda_{\alpha n}}{\partial c}, \quad \frac{\partial \lambda_{\beta n}}{\partial c} \quad \text{and} \quad \frac{\partial \gamma_n}{\partial c}.$$

It is also noted

that in order to compute $\frac{\partial F}{\partial X_n}$ and $\frac{\partial F}{\partial X_0}$, in particular, we

need $\frac{\partial \lambda_{\alpha n}}{\partial \alpha_n}$, $\frac{\partial \lambda_{\beta n}}{\partial \beta_n}$, $\frac{\partial \gamma_n}{\partial \beta_n}$, $\frac{\partial T^*}{\partial \alpha_0}$, $\frac{\partial T^*}{\partial \rho_0}$, and $\frac{\partial T^*}{\partial d_0}$. Since

$$\frac{\partial \lambda_{\alpha n}}{\partial c}, \quad \frac{\partial \lambda_{\beta n}}{\partial c}, \quad \frac{\partial \gamma_n}{\partial c} \quad \text{and terms necessary to compute} \quad \frac{\partial F}{\partial X_n}$$

and $\frac{\partial F}{\partial X_0}$ are simple to calculate they are not discussed here.

From the above discussion, it becomes clear that in order to compute phase-velocity partial derivatives with respect to model parameters, we need only to compute $\frac{\partial (a_m)_{ij}}{\partial X_m}$, $\frac{\partial (a_m)_{ij}}{\partial c}$

and $\frac{\partial T^*}{\partial c}$. The expressions for these terms are given in the Appendix.

The merit of the present method may lie in the simplicity of the algorithm. Equations (4) and (6) in connection with dispersion equation (2) explain essentially all procedures required. Partial derivatives of layer-matrix elements given in the Appendix provide expressions needed in the computation of (4) and (6).

6. Generalized Linear Inversion

The generalized linear inversion method, which may be viewed as a discrete specialization of the general formulation of the Backus-Gilbert inversion technique (Backus and Gilbert, 1967, 1968, 1970), has been applied to geophysical problems in many previous studies (Smith and Franklin, 1969; Der et al., 1970; Parker, 1970; Wiggins, 1972; Jackson, 1972; Ward et al., 1973; Braile et al., 1974; Braile and Keller, 1975; Pedersen, 1977, among others). The inversion scheme used in this study closely follows the algorithm described by Wiggins (1972) and Jackson (1972). However, an outline of the method along with some points relevant to the present study are given below.

In general geophysical inversion problems, we have a nonlinear system dealing with n observations and m model parameters. In the following we shall use the subscript i to represent the i th observation and the subscript j to designate the j th parameter. We shall use a small letter to represent a scalar, a small letter with a bar underneath it a vector,

and a capital letter a matrix.

The earth model we assume must be capable of providing us with a functional relationship between the model parameters and the calculated values. The model parameters will be represented by a vector such that

$$\underline{x} = (\alpha, \beta, \rho, d)$$

where α , β , ρ and d are functions of depth. The calculated values represent the group velocity and will be designated by $y(x)$. We expand the problem functional $y(x)$ in a Taylor series about an initial model x_0 :

$$\begin{aligned} y_i(x) &= \sum_{k=0}^{\infty} \frac{y_i^{(k)}(x_0)}{k!} (x - x_0)^k \\ &= y_i(x_0) + \left. \frac{\partial y_i(x)}{\partial x_j} \right|_{x=x_0} \cdot (x - x_0) + \epsilon [(x - x_0)^k], \quad k \geq 2 \quad (7) \end{aligned}$$

where $\epsilon [(x - x_0)^k]$ is the functional in the second or higher ($k \geq 2$) order terms in $(x - x_0)$. We linearize the problem by retaining the linear part and neglecting the nonlinear part of (7). By setting

$$\begin{aligned} \delta x_j &= x_j - x_{0j} \\ \delta y_i &= y_i(x) - y_i(x_0) \\ A_{ij} &= \frac{\partial y_i}{\partial x_j} \end{aligned} \quad (8)$$

(7) becomes

$$\underline{\delta y} = A \underline{\delta x} \quad (9)$$

Hence we have a linear system in n equations and m unknowns and the systems Matrix A is, in general, not square.

Equation (8) may be viewed as follows: X_j represents the true earth, X_{0j} the initial model, δX_j the correction to be made to the initial model; $y_i(X)$ represents the observed group velocity at the i th period, $y_i(X_0)$ the group velocity for the i th period computed from the initial model, δy_i the difference in group velocity between the model and the true earth. It is noted that the expansion of the problem functional in Taylor series is based on the assumption that the group velocity is a smoothly varying function of the parameters. Also the linearization is justified only for small values of the parameter corrections δX_j . If δX_j must be large to satisfy the observations, then the results must be checked by expanding the functional about a new initial model.

For simplicity in notation, we replace \underline{x} for $\underline{\delta x}$ and \underline{y} for $\underline{\delta y}$, while keeping in mind that \underline{x} and \underline{y} actually represent $\underline{\delta x}$ and $\underline{\delta y}$, respectively. Then (9) becomes

$$A \underline{x} = \underline{y} \quad (10)$$

If we can find A^{-1} , the exact inverse of A , then we can solve the system for \underline{x} . But since A is, in general, not square, and possibly singular even when it is square, the

inverse of A does not exist. The generalized linear inversion is a way of avoiding this difficulty by finding the best possible approximation to a matrix of quantities, which may be conceivably called the exact inverse of A and designated by A^{-1} . This procedure may be conceptualized in the following way.

First consider the adjoint system of (10):

$$A^T \underline{x}' = \underline{y}' \quad (11)$$

where the superscript T represents the transpose of the matrix. The combination of (10) and (11) into an identity gives

$$\begin{bmatrix} 0 & A \\ A^T & 0 \end{bmatrix} \begin{bmatrix} \underline{x}' \\ \underline{x} \end{bmatrix} = \begin{bmatrix} \underline{y} \\ \underline{y}' \end{bmatrix} \quad (12)$$

It is noted that the matrix in (12), whose blocks consist of A , A^T and 0 , is symmetric and its size is $(n+m) \times (n+m)$. We shall call this symmetric matrix S . Let us consider the eigenvalue problem for S :

$$S \underline{w} = \lambda \underline{w} \quad (13)$$

The component of \underline{w} may be separated into contributions from the n -dimensional data space of group velocities and the m -dimensional parameter space such that

$$\underline{w}^T = (u_1, u_2, \dots, u_n, v_1, v_2, \dots, v_m) \quad (14)$$

Then (13) may be expressed as

$$\begin{bmatrix} 0 & A \\ A^T & 0 \end{bmatrix} \begin{bmatrix} \underline{u} \\ \underline{v} \end{bmatrix} = \lambda \begin{bmatrix} \underline{u} \\ \underline{v} \end{bmatrix} \quad (15)$$

That is,

$$\begin{aligned} A \underline{v} &= \lambda \underline{u} \\ A^T \underline{u} &= \lambda \underline{v} \end{aligned} \quad (16)$$

From (16) we obtain

$$\begin{aligned} A^T A \underline{v} &= \lambda^2 \underline{v} \\ A A^T \underline{u} &= \lambda^2 \underline{u} \end{aligned} \quad (17)$$

Let

$$\mu = \lambda^2; \quad B = A^T A; \quad C = A A^T \quad (18)$$

Then (17) becomes

$$\begin{aligned} B \underline{v} &= \mu \underline{v} \\ C \underline{u} &= \mu \underline{u} \end{aligned} \quad (19)$$

From either of the standard eigenvalue problems (19), in connection with (16), we can find λ , \underline{u} and \underline{v} .

Since B and C are symmetric, u_i and v_j form sets of orthogonal vectors. Let

$$q = \text{rank}(B) = \text{rank}(C) \quad (20)$$

Then

$$q \leq \min(n, m) \quad (21)$$

We normalize u_i and v_j and define matrices U_g and V_g such that the columns consist of u_i , $i=1, g$; and v_j , $j=1, g$; respectively, and define a diagonal matrix Λ_g whose diagonal elements are λ_k , $k=1, g$ arranged in decreasing order.

Then we realize the following:

(i) Always

$$U_g^T U_g = I_g; \quad V_g^T V_g = I_g \quad (22)$$

where a subscript of I indicates the size of the identity matrix. Equation (22) is true since the multiplication in (22) always involves the inner product of orthonormal eigenvectors.

(ii) When $g = n < m$, i.e., the system is under-determined,

$$U_g U_g^T = I_n = I_g \quad (23)$$

and this condition guarantees the existence of a solution (Jackson, 1972).

(iii) When $g = m < n$, i.e., the system is over-determined,

$$V_g V_g^T = I_m = I_g \quad (24)$$

and this condition guarantees the uniqueness of the solution, if a solution to the problem exists (Jackson, 1972).

(iv) When $g = n = m$, i.e., the system is even-determined,

$$U_g U_g^T = V_g V_g^T = I_g$$

and this condition guarantees the existence and uniqueness of a solution.

With U_g , V_g and Λ_g so defined, we obtain from the first equation of (16) that

$$A = U_g \Lambda_g V_g^T \quad (25)$$

Substituting (25) into (10) gives

$$U_g \Lambda_g V_g^T \underline{x} = \underline{y}$$

from which we obtain

$$V_g V_g^T \underline{x} = V_g \Lambda_g^{-1} U_g^T \underline{y} \quad (26)$$

Let

$$R = V_g V_g^T \quad (27)$$

Then

$$R \underline{x} = V_g \Lambda_g^{-1} U_g^T \underline{y} \quad (28)$$

Let

$$\hat{\underline{x}} = R \underline{x} \quad (29)$$

Then

$$\hat{\underline{x}} = V_g \Lambda_g^{-1} U_g^T \underline{y} \quad (30)$$

From (24) and (28), it is noted that if $g = m < n$, then R becomes I_m and (28) gives a unique solution \underline{x} , which is identical to $\hat{\underline{x}}$; that if $g \neq m$, then the degree of likeness of R to I gives the degree of uniqueness of our estimated solution $\hat{\underline{x}}$. Due to this property of R , it is called the resolution matrix, and its rows are called resolving kernels.

Let

$$H = V_g \Lambda_g^{-1} U_g^T \quad (31)$$

Then (30) becomes

$$\hat{\underline{x}} = H \underline{y} \quad (32)$$

from which it is easily understood that H bears the nature of the inverse of A , through which we could find the best estimate of the solution \hat{x} . Due to this characteristic of H , it is called the generalized linear inverse of A .

From the viewpoint of the above discussion, (10) may be viewed in the following two ways:

$$A \underline{x} = \underline{y}^o \quad (33)$$

$$A \hat{x} = \underline{y}^p \quad (34)$$

where the superscripts o and p represent the observed and predicted (calculated from the earth model) data, respectively. From this point of view, (32) may be expressed as

$$\hat{x} = H \underline{y}^o \quad (35)$$

Substituting (35) into (34) gives

$$\underline{y}^p = A H \underline{y}^o \quad (36)$$

Again substituting (25) and (31) into (36) gives

$$\underline{y}^p = U_g U_g^T \underline{y}^o \quad (37)$$

Let

$$D = U_g U_g^T \quad (38)$$

Then

$$\underline{y}^p = D \underline{y}^o \quad (39)$$

From (23) and (37), it is noted that if $g = n < m$, then D becomes I_n and (37) tells us that the estimated solution is exact in the sense that the predicted and observed data are identical; that if $g \neq n$, then the degree of likeness of D to I gives the degree of independence of the observed data. Due to this characteristic of D , it is called the information density matrix.

7. Propagation of Errors

Lastly we wish to know how the uncertainty of our observations affects the solution of the problem presented by (10), which is an error-free system. Since we have a certain amount of uncertainty or error, $\underline{\epsilon}$, in the observed data, (10) may be, in this system with erroneous data, expressed as

$$\underline{\epsilon} = A \underline{x} - \underline{y} \quad (40)$$

Then the best estimate, $\hat{\underline{x}}$, of the true solution \underline{x} , is the solution which minimizes the square error

$$\underline{\epsilon}^T \underline{\epsilon} = (A \underline{x} - \underline{y})^T (A \underline{x} - \underline{y}) \quad (41)$$

In general, different data may have different reliability and/or different units. In order to take this into account, we wish to give different weights to different data. From the fundamental theory of statistics we know that the optimal weighting matrix for this purpose is the inverse of the data covariance matrix. Therefore instead of minimizing (41), we minimize

$$\underline{\epsilon}^T C^{-1} \underline{\epsilon} = (A \underline{x} - \underline{y})^T C^{-1} (A \underline{x} - \underline{y}) \quad (42)$$

where C is the covariance matrix of data. Differentiating (42) with respect to \underline{x}^T and setting it equal to zero gives

$$\hat{\underline{x}} = (A^T C^{-1} A)^{-1} A^T C^{-1} \underline{y} \quad (43)$$

Thus we have obtained the best estimate $\hat{\underline{x}}$ of the true solution \underline{x} for a given level of error in the data.

Hamilton (1964) has shown that under the above circumstances the following holds:

$$\text{cov}(\hat{\underline{x}}) = (A^T A)^{-1} \sigma_y^2 \quad (44)$$

where $\text{cov}(\hat{\underline{x}})$ is the covariance matrix of the model parameters, and σ_y^2 is the variance of the data. Substituting (25) into (44) for our generalized linear inverse formalism gives

$$\text{cov}(\hat{\underline{x}}) = V_g \Lambda_g^{-2} V_g^T \quad (45)$$

Hence the variance of our model parameters may be expressed as

$$(\sigma_x^2)_j = \sum_{k=1}^g \frac{V_{jk}^2}{\lambda_k^2} \sigma_y^2, \quad j = 1, m \quad (46)$$

8. Consideration for Model Parameters with Different Dimensions

Since in the present problem, we have model parameters α , β , ρ and d which have different units and sizes, we wish to account for this property of our set of model parameters.

Smith and Franklin (1969) have shown that the generalized linear inversion of the system (10) simultaneously minimizes both

$$\underline{\epsilon}^T \underline{\epsilon} = (\underline{A} \underline{x} - \underline{y})^T (\underline{A} \underline{x} - \underline{y}) = \|\underline{A} \underline{x} - \underline{y}\|^2 \quad (41)$$

and

$$\underline{x}^T \underline{x} = \|\underline{x}\|^2 \quad (47)$$

In other words, the generalized linear inverse selects the smallest variation \underline{x} of the parameters that will satisfy the system of simultaneous linear equations (10).

In order to account for the different dimensions or sizes of the model parameters, we introduce the inverse of the parameter covariance matrix, W^{-1} , as a weighting matrix. Wiggins (1972) has shown that this choice of weighting has the interesting and convenient property of making the lengths of the rows of $AW^{1/2}$ invariant to the selection of layer thicknesses. Now we want to simultaneously minimize

$$\underline{\epsilon}^T C^{-1} \underline{\epsilon} \quad (42)$$

and

$$\underline{x}^T W^{-1} \underline{x} \quad (48)$$

instead of (41) and (47).

In order to simplify the process, we introduce the transformation of Wiggins (1972) and Jackson (1972):

$$A^* = C^{-1/2} A W^{1/2} \quad (49)$$

$$\underline{x}^* = W^{-1/2} \underline{x} \quad (50)$$

$$\underline{y}^* = C^{-1/2} \underline{y} \quad (51)$$

When we consider the system

$$A^* \underline{x}^* = \underline{y}^* \quad (52)$$

$$\underline{\epsilon}^* = A^* \underline{x}^* - \underline{y}^* \quad (53)$$

we find that

$$\underline{\epsilon}^{*T} \underline{\epsilon}^* = \underline{\epsilon}^T C^{-1} \underline{\epsilon} \quad (54)$$

$$\underline{x}^{*T} \underline{x}^* = \underline{x}^T W^{-1} \underline{x} \quad (55)$$

Thus we have shown that with transformations (49) to (51), minimizing $\underline{\epsilon}^{*T} \underline{\epsilon}^*$ and $\underline{x}^{*T} \underline{x}^*$ is equivalent to minimizing $\underline{\epsilon}^T C^{-1} \underline{\epsilon}$ and $\underline{x}^T W^{-1} \underline{x}$. Therefore we take the convenience of doing the former.

RESULTS AND DISCUSSION

The corrections for the phase response of both the old and new instruments are shown in Table 3. Both the period and corrections are in units of seconds.

Der et al. (1970) have shown that when group-velocity dispersion observation points are evenly spaced on a logarithmic period scale, each of the chosen data points furnishes approximately the same amount of information about the subsurface. In other words, this choice of observation periods provides the greatest independence of data with the same number of observation points. In the present study, observation points were chosen at approximately equally spaced intervals on a logarithmic period scale with the interval such that $\Delta (\log T) \approx 0.1$ in the range from 10 to 100 sec. This choice of interval or the number of observation points was guided by inspection of the shape of partial-derivative curves obtained in preliminary studies of the structure of the area. The periods indicated in Table 3 represent those observation periods so determined.

The corrections for the sphericity and gravity of the earth are shown in Table 4. The values in Table 4 were weighted in proportion to the path lengths corresponding to different provinces as indicated in Table 2; they were subtracted from the observed group velocities. As noted from

TABLE 3
ALPHA INSTRUMENT CORRECTIONS IN SEC

Period	10	13	16	20	25	32	40	50	64	80
Old Instrument	3.250	5.249	7.999	11.998	16.676	20.048	22.480	24.000	25.022	26.017
New Instrument	3.092	4.998	6.505	8.475	10.250	13.000	16.200	19.677	23.780	27.015

TABLE 4
SPHERICITY CORRECTIONS IN KM/SEC

Period	10	13	16	20	25	32	40	50	64	80
Continental										
Alaska	0.001	0.001	0.001	0.001	0.001	0.002	0.003	0.004	0.007	0.010
Bering Shelf	0.001	0.001	0.002	0.002	0.003	0.005	0.007	0.009	0.012	0.014
Aleutian Basin	0.002	0.003	0.003	0.004	0.005	0.006	0.008	0.009	0.011	0.014

Table 4, the corrections are so small that they are less than the uncertainty of the observed data discussed previously. However, since they provide a systematic change in group velocity, these corrections were applied to the observed data.

The observed group velocity dispersion curves determined from the phase-matched filtering and corrected as discussed above are shown in Fig. 5. In comparison with dispersion curves of an average earth (e.g. Oliver, 1962; to avoid confusion due to crowded curves, they are not shown in Fig. 5), the following is observed. The dispersion curve obtained for continental Alaska (event 0509) is similar to that of the average continental earth of Oliver (1962) except that it has slightly higher velocities in the longer periods and lower velocities in the shorter periods. For epicenters farther to the west along the Aleutian Islands, the dispersion curves shift toward that of the average oceanic earth of Oliver (1962) but the velocity values are still much closer to that of the average continental earth than to the average oceanic earth.

The results of the inversion of the group-velocity dispersion relationships are described in the following paragraphs. In the inversion scheme used here, since there is no way to predict precisely the variance of parameters, a constant value of 0.15 was used as an initial estimate of the standard deviation of parameters.

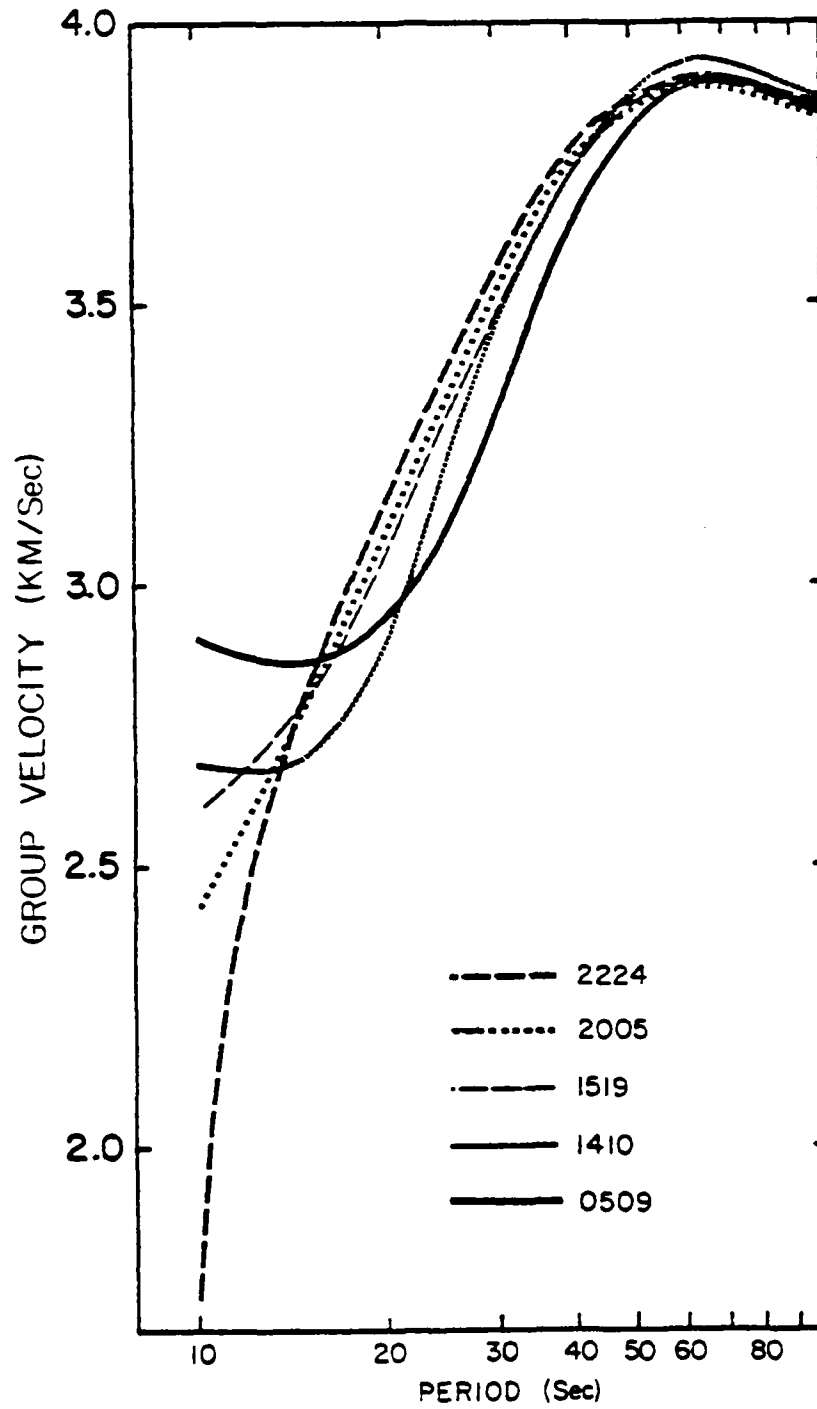


Figure 5: Observed Group Velocity Dispersion of the Events Used

1. Continental Alaska

The initial model for the structure of continental Alaska is shown in Table 5. In constructing initial models, the updated comprehensive parametric earth models of Dziewonski et al. (1975) were frequently consulted. Stacey (1977) gives these models as representative earth models in his recent textbook.

Although the method developed in this study and the computer code used to implement the method are capable of computing the group-velocity partial derivatives with respect to thickness of the layers, for the sake of simplicity and convenience, the thicknesses of the layers were held fixed and parameters β , ρ and α within each layer were corrected in the inversion process.

Partial derivatives of the group velocity with respect to β , ρ and α are shown in Figs. 6, 7 and 8, respectively. The numbers on curves designate the corresponding layers. It is noted from the figures, as expected, that partial derivative maxima shift toward longer periods as the depths of the layer increase. It is also noted that the amplitudes of the β partial derivatives are significantly greater than those of the other partials and that the α partials are the least significant of all.

The structure of the final model for this region obtained from the Alaskan event is shown in Fig. 9. Also shown in the figure are standard deviations of the model parameters indicated by horizontal bars at the center of each layer.

TABLE 5
INITIAL MODEL FOR CONTINENTAL ALASKA

<u>Layer</u>	<u>P-velocity (km/sec)</u>	<u>S-velocity (km/sec)</u>	<u>Density (g/cm³)</u>	<u>Thickness (km)</u>	<u>Depth to Bottom of Layer (km)</u>
1	3.670	2.310	2.320	0.8	0.8
2	5.411	3.266	2.637	2.1	2.9
3	5.789	3.453	2.768	6.1	9.0
4	6.152	3.483	2.800	7.0	16.0
5	6.398	3.617	2.848	7.0	23.0
6	6.490	3.894	2.962	10.0	33.0
7	6.687	4.024	2.984	10.0	43.0
8	8.016	4.649	3.325	20.0	63.0
9	8.021	4.666	3.333	50.0	113.0
10	7.853	4.461	3.387	50.0	163.0
11	7.853	4.468	3.388	50.0	213.0
12	8.651	4.652	3.452		

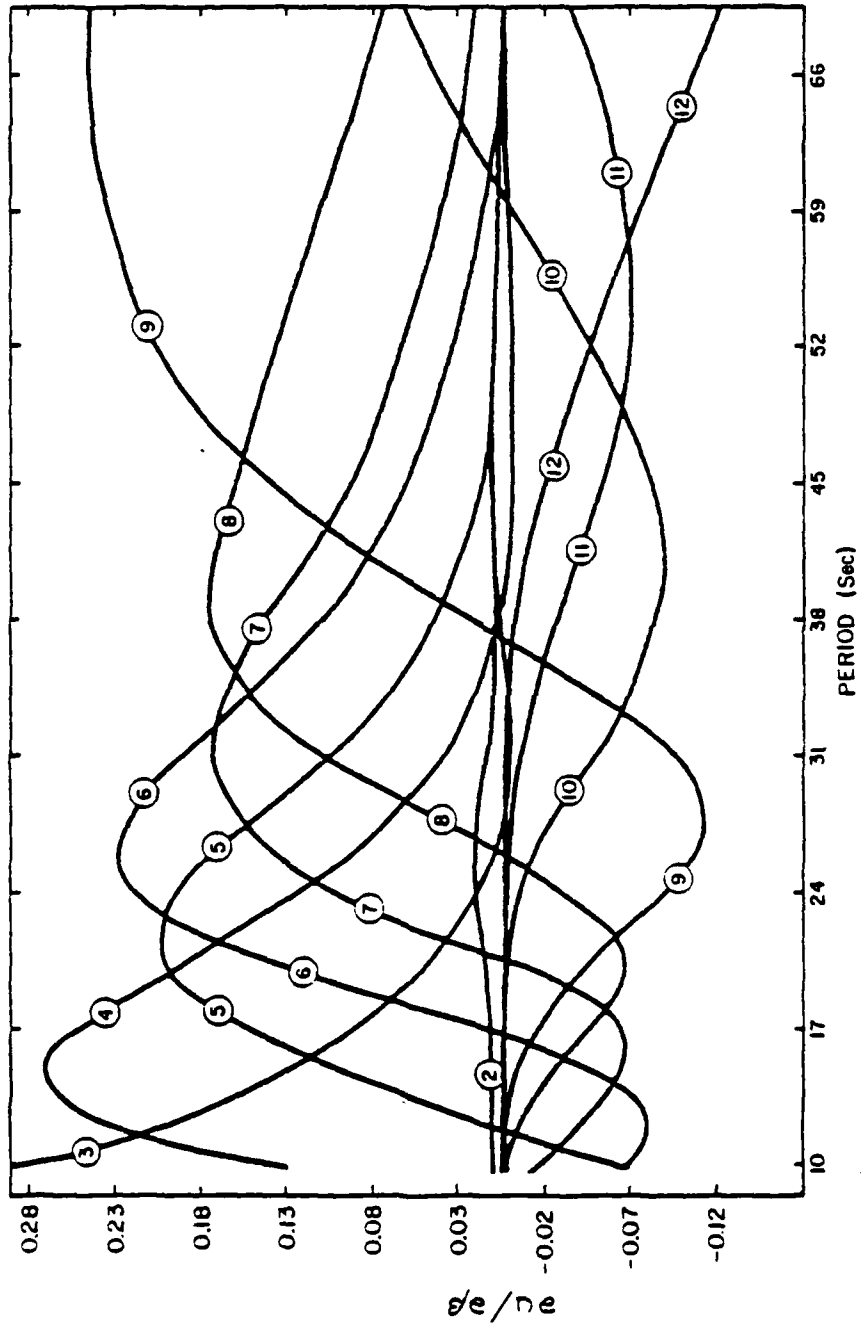


Figure 6: Group Velocity Partial Derivatives with Respect to Shear Velocity in Alaska

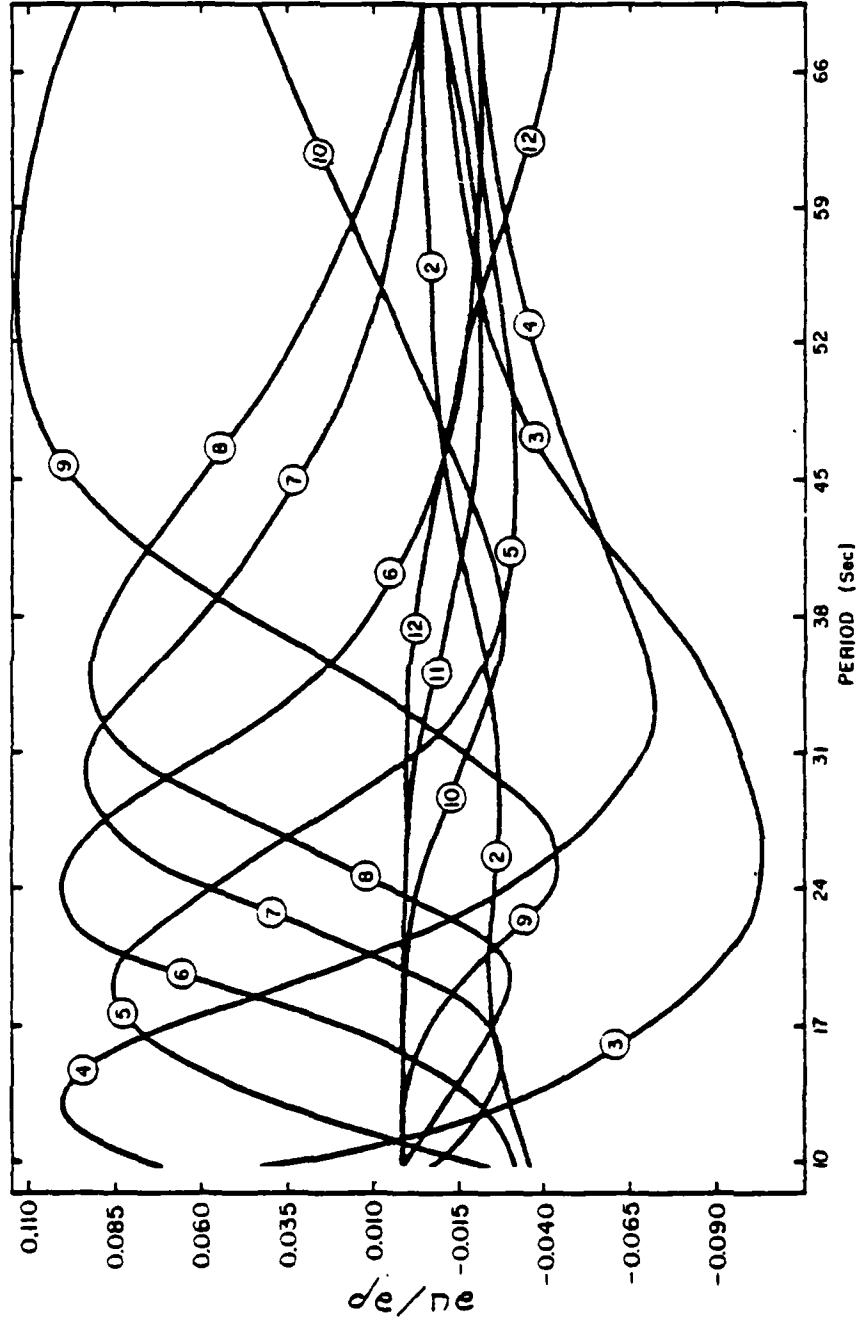


Figure 7: Group Velocity Partial Derivatives with Respect to Density in Alaska

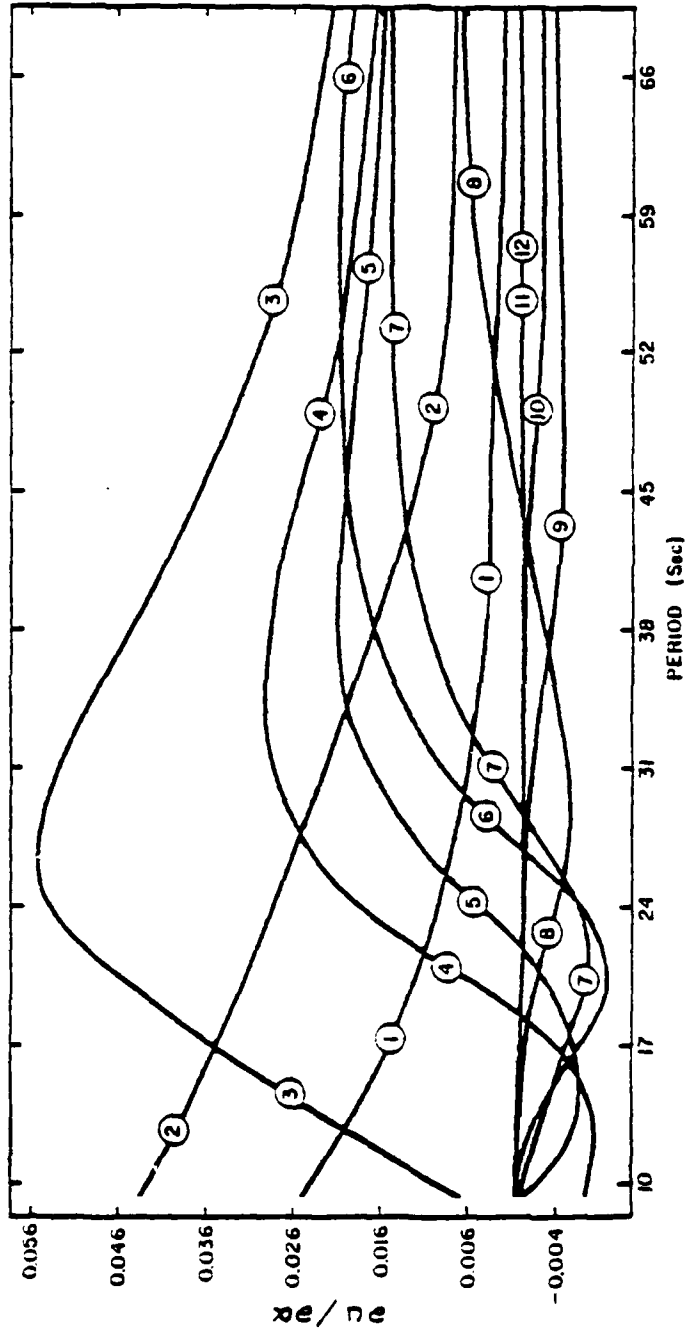


Figure 8: Group Velocity Partial Derivatives with Respect to Compressional Velocity in Alaska

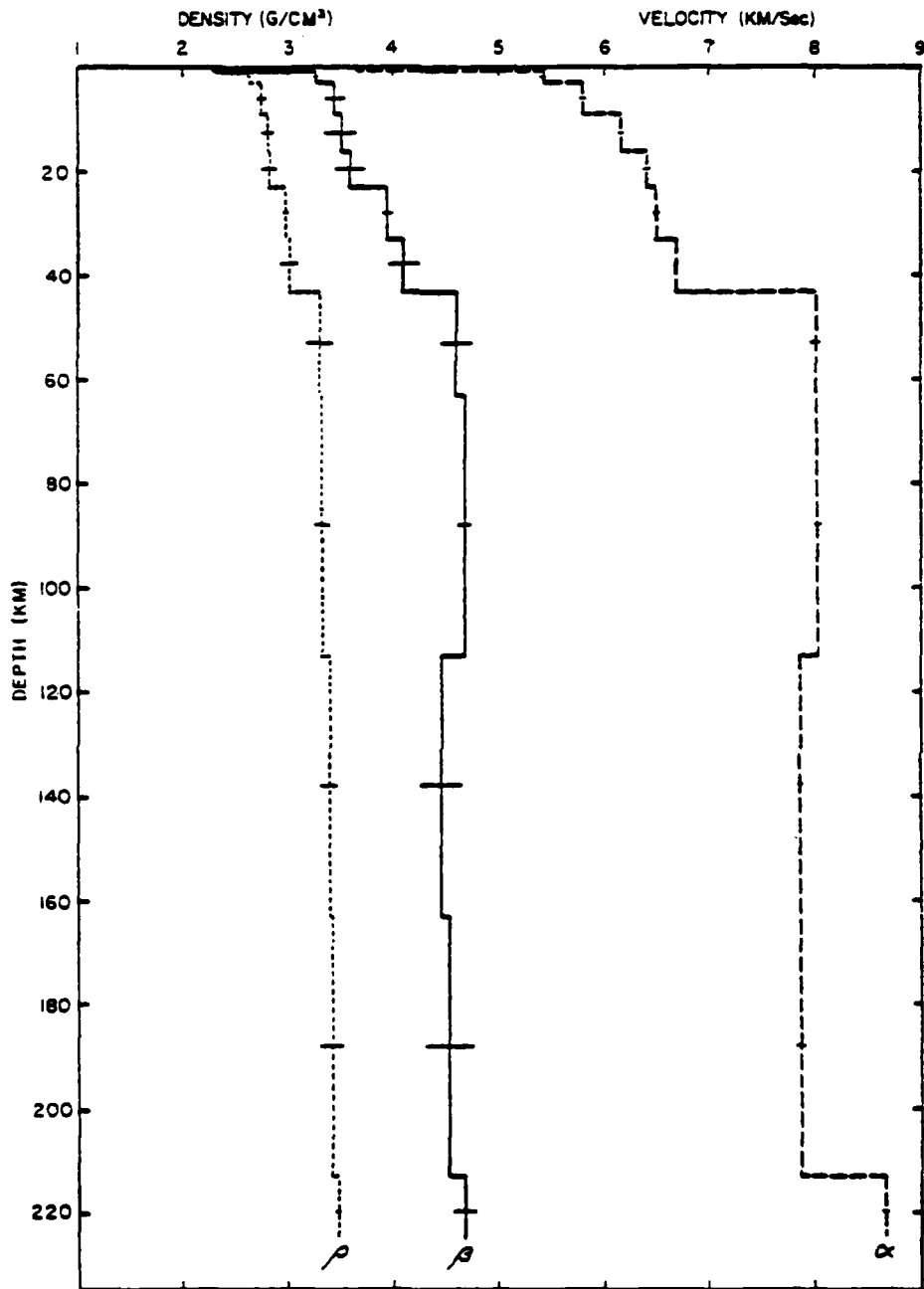


Figure 9: Structure of the Final Model for Continental Alaska

The greatest estimated standard deviation of parameters was 0.28 km/sec for the shear velocity of the layer centered at a depth of 188 km. The observed and predicted group velocities are shown in Fig. 10. The rms error of the predicted values against the observed ones was 0.02 km/sec, which is less than the uncertainty of the data. The differences between the observed and predicted values were all within the standard deviation of the data except at the period of 25 sec, where the difference was 0.04 km/sec.

It is observed from Fig. 9, and also from Figs. 16 and 23 for the other regions as shown later, that the magnitude of the standard deviations of model parameters decreases from β to ρ and to α . These trends do not appear to represent the real accuracy of the model, for from the physical point of view, α would have about the same as or possibly greater uncertainty than β . Therefore this apparent differential accuracy among the parameters is interpreted to be caused by some property of the present generalized linear inversion method. A possible explanation is given below. As an initial estimate of standard deviation of parameters, we used 0.15 for all parameters. Since the values of partial derivatives of the group velocity with respect to α are much smaller than those of ρ , and still smaller than those of β , while a constant initial estimate of standard deviation was used for all parameters, less flexibility in parameter correction seems to have been given to ρ and still less to α in order for the system to find a new model which fits the observed data better

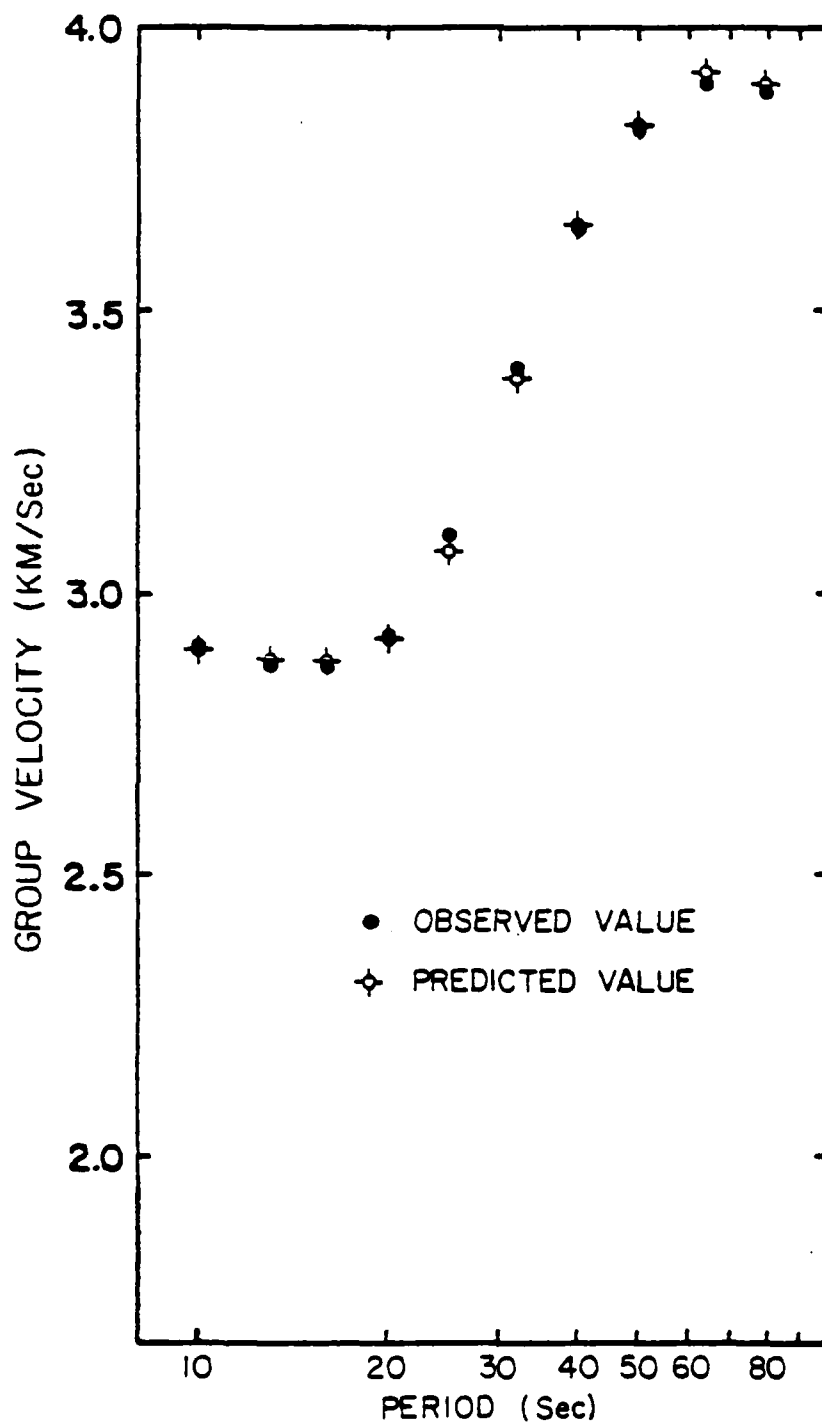


Figure 10: Observed and Predicted Group Velocities for Continental Alaska

than the initial model. In other words, smaller allowance or variance for ρ and α relative to β was required by the system in making correction to the model. Therefore the apparent smaller standard deviations for ρ and α are attributed to estimation error rather than to greater accuracy in determining parameters ρ and α . A better initial estimate of the covariance matrix of model parameters may resolve this problem.

Two features of the structure worth noticing from Fig. 9 are the depth to the Mohorovicic discontinuity and the presence of the low velocity zone (LVZ). The depth to the Moho is 43 km. Although no previous studies, to this author's knowledge, have been conducted covering the same area as the present one, the thickness of the crust obtained here may be compared with results of other studies made in areas nearby. Using gravity data, Woollard et al. (1960) estimated the crustal thickness near Fairbanks to be about 33 km. Hales and Asada (1966) gave 48 to 53 km, estimated from their seismic refraction studies, as the depth to the Moho for the area from College Fiord to the northeast, which is near Fairbanks. Hanson et al. (1968) found from their seismic refraction interpretation that the Moho is at a depth of 32 km under Fairbanks and 48 km under their shot point, which is about 120 km southwest of Fairbanks. The present model is essentially in agreement with the refraction results of Hanson et al. (1968) in the structure of the top 10 km, except that their model has a layer of sediments a little thicker than in

the present model. Since their model has only a few layers, the present model cannot be checked with their results in the deeper structure.

From Fig. 9 it is also noted that a LVZ is present in the region and it extends from the depth of about 113 to 213 km. The presence and depth range of the LVZ of the present model is in essential agreement with the parametric continental model of Dziewonski et al. (1975).

Resolving kernels for β and ρ of the final model for this region are shown in Figs. 11 and 12, respectively. Depth corresponding to each resolving kernel is indicated in the figures. Some sidelobes and deviation of the resolution matrix from an identity matrix are observed in the resolving kernels for β . The sidelobes and deviation are seen to have worsened in the case of ρ . The resolving kernels for α in this and the other regions were so irregular in shape that they were not plotted.

Also shown for the bottom layer of the crust in Fig. 11 is the spread, which is the depth range of the rectangle which has the same area as that under the associated resolving kernel. Since the spread for this layer is 16 km compared with a 10 km thickness of the layer, the uncertainty of the depth to the Moho is interpreted to be ± 3 km. Therefore a reasonable value for the thickness of the crust in this region is 43 ± 3 km, where 43 km is the depth to the bottom of the lowest layer in the crust. Although the corresponding spread for ρ is comparable to that for β , since β is the most

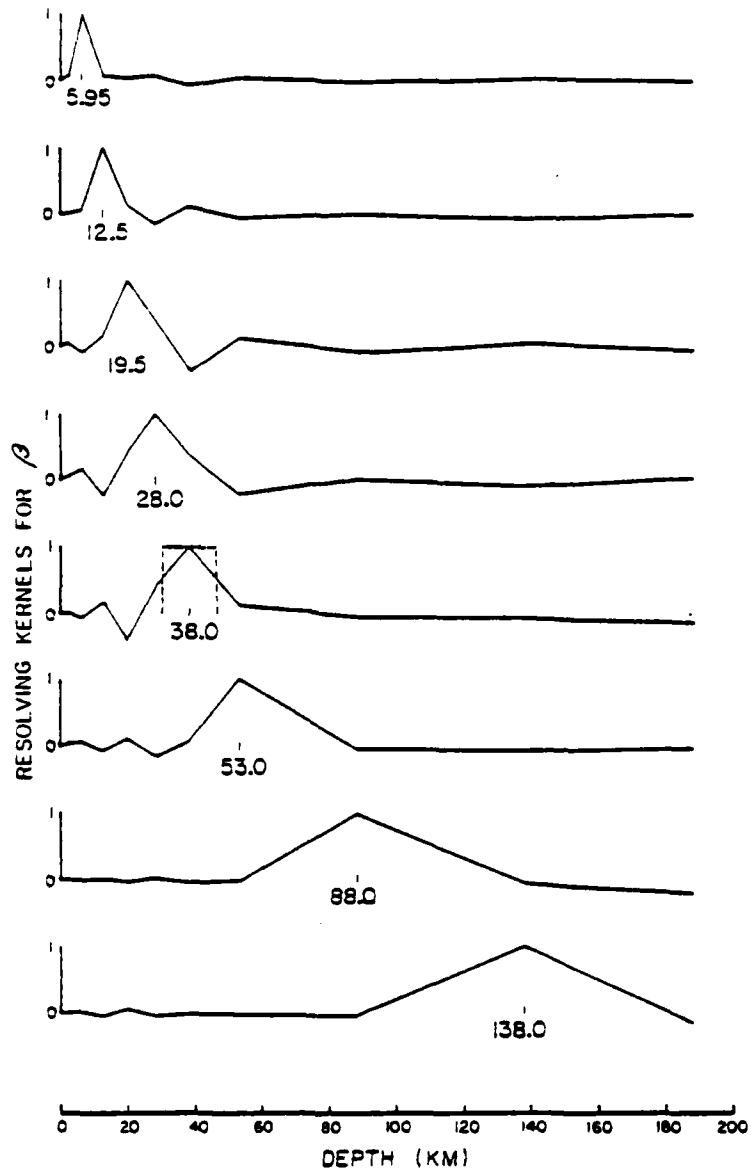


Figure 11: Resolving Kernels for Shear Velocity in Continental Alaska

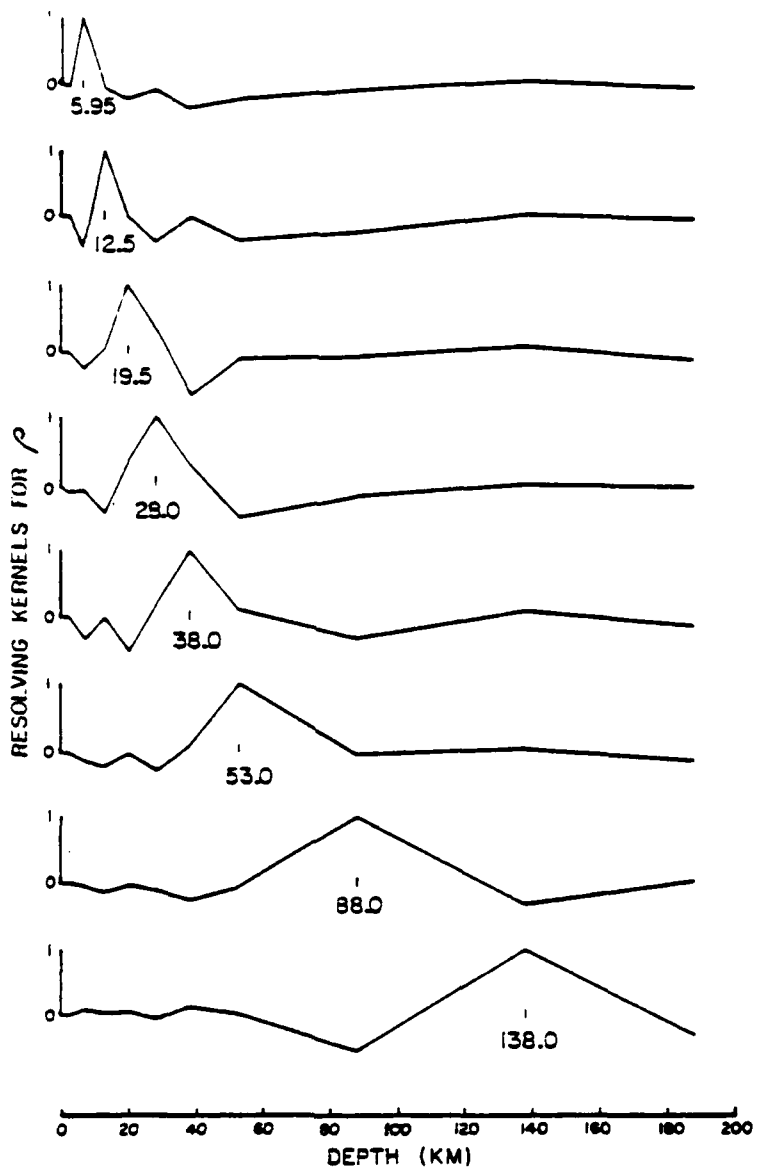


Figure 12: Resolving Kernels for Density in Continental Alaska

influential parameter in the inversion and its resolving kernels look most reliable in the sense that they show least sidelobes, the spread is shown only for β .

The information density distributed in the model for this region is shown in Fig. 13. It is noted from the figure that the information density matrix has to some extent been degraded, i.e. distorted from the identity matrix. This degree of distortion is, however, considered desirable. If the information density matrix is a perfect identity matrix, although the economy of data acquisition and processing is optimal, there always exists a possibility of missed information needed in the inversion. On the other hand, if the information density matrix is too severely distorted, it may guarantee that sufficient information may have been propagated into the inversion process, but the economy of data acquisition and processing suffers severely. Although the desirable degree of distortion of the information density matrix is difficult to determine quantitatively and consequently is a subjective matter, that degree of distortion which appears in Fig. 13 is considered a reasonable compromise.

2. Bering Shelf

The initial model for the Bering Shelf region is shown in Table 6. Group-velocity partial derivatives with respect to the three parameters for this region are shown for periods 25 and 40 sec in Figs. 14 and 15, respectively. As expected, the partial derivative maxima and minima are shifted to

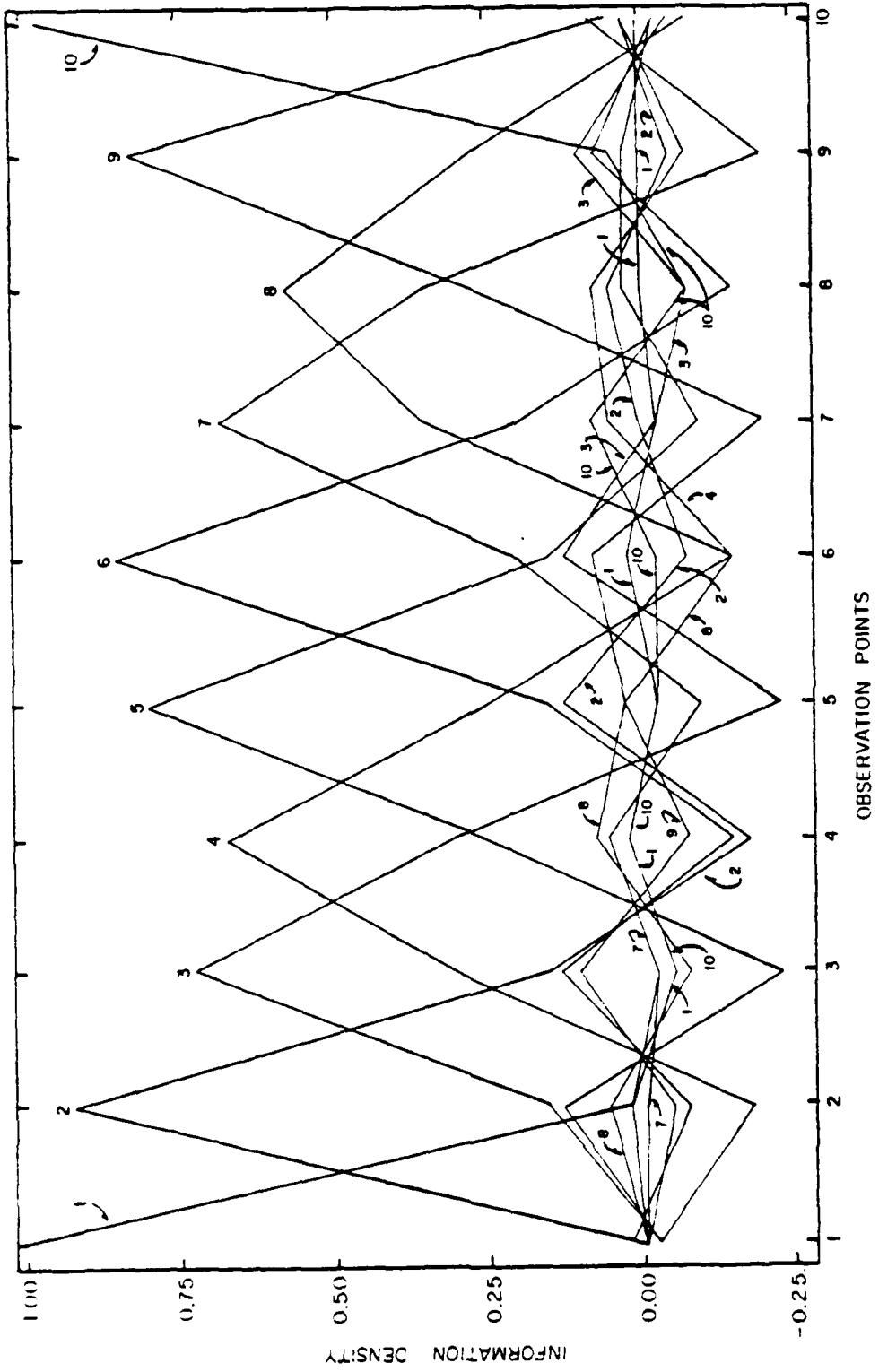


Figure 13: Information Density in Continental Alaska

TABLE 6
INITIAL MODEL FOR THE BERING SHELF

<u>Layer</u>	<u>P-velocity (km/sec)</u>	<u>S-velocity (km/sec)</u>	<u>Density (g/cm³)</u>	<u>Thickness (km)</u>	<u>Depth to Bottom of Layer (km)</u>
0	1.520	0.000	1.030	0.1	0.1
1	2.000	1.000	1.500	1.0	1.1
2	3.670	2.310	2.320	2.3	3.4
3	5.789	3.453	2.768	4.2	7.6
4	6.152	3.483	2.800	7.0	14.6
5	6.393	3.617	2.848	7.0	21.6
6	6.490	3.894	2.962	6.0	27.6
7	7.934	4.654	3.310	10.0	37.6
8	8.016	4.649	3.325	20.0	57.6
9	8.021	4.666	3.333	50.0	107.6
10	7.853	4.461	3.387	50.0	157.6
11	7.853	4.468	3.388	55.0	212.6
12	8.651	4.652	3.452		

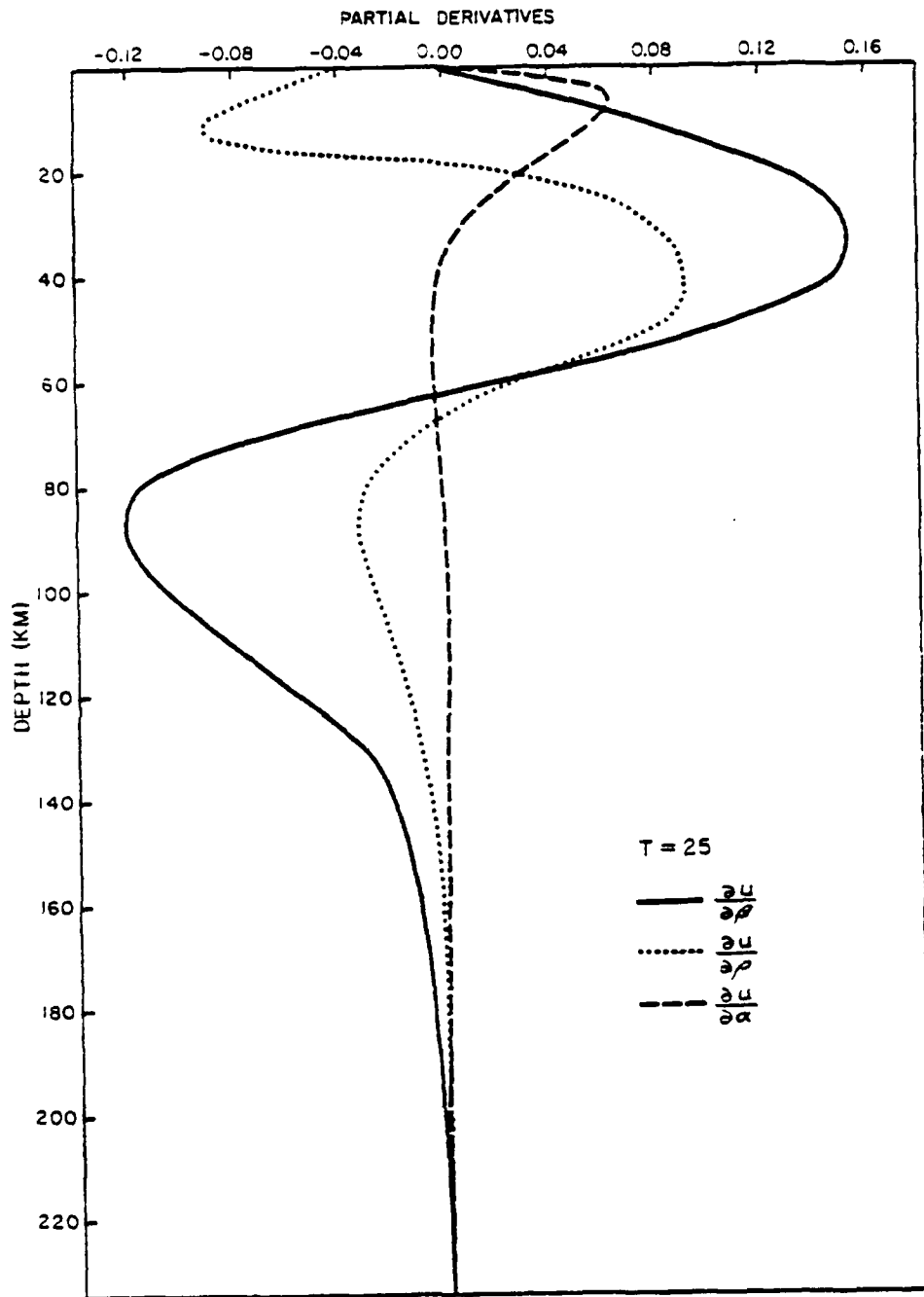


Figure 14: Group Velocity Partial Derivatives for $T=25$ in the Bering Shelf

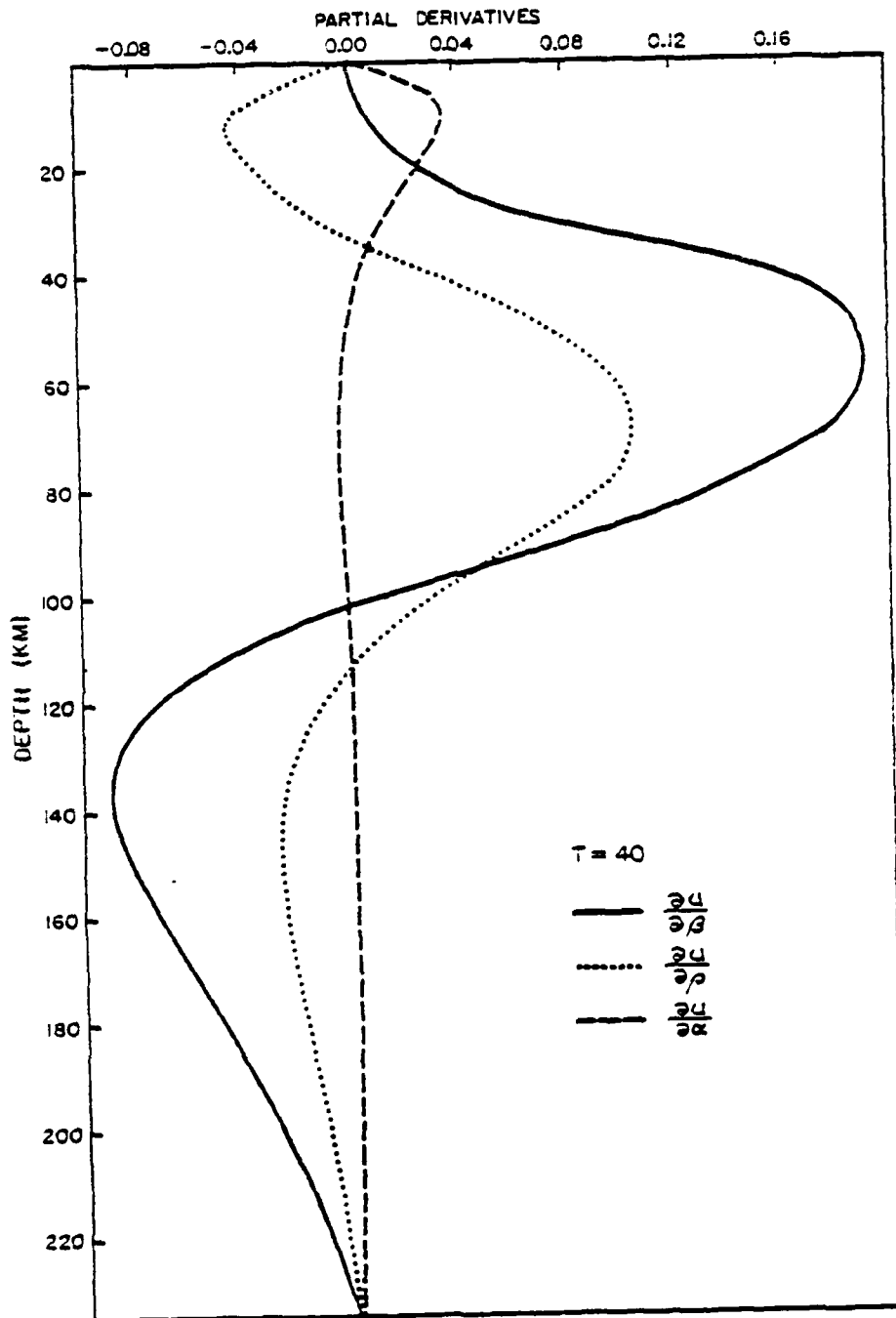


Figure 15: Group Velocity Partial Derivatives for T=40 in the Bering Shelf

greater depths as the period increases. It is also noted from these figures and Figs. 21 and 22 as shown later, that the amplitude of density partial derivatives relative to that of shear velocity partial derivatives decreases with depth.

The structure of the final model for this region derived from the analysis of event 1410, along with the standard deviations of the parameters, is shown in Fig. 16. The greatest standard deviation was 0.29 km/sec for shear velocity of the layer centered at a depth of 133 km. The observed and predicted group velocities are shown in Fig. 17. All the differences between the observed and predicted values and their rms error were within the uncertainty of the data.

It is seen from Fig. 16 that the depth to the Moho is 27.6 km. This value may be compared with 29 km estimated from seismic refraction studies of Shor (1964) in the southwestern part of the Bering Shelf (stations MK11 and MK12 of Shor, 1964). Also the thicknesses and velocities of surface layers are in reasonable agreement with those of Shor (1964). Since Shor's model has only a few layers, the deeper layers cannot be checked against the refraction results. Also noted from Fig. 16 is the existence of a LVZ which ranges from about 108 km to about 213 km in depth. This depth range of the LVZ may be comparable to the earth model averaged over the whole earth including oceans and continents, of Dziewonski et al. (1975).

Resolving kernels for β and ρ along with the corresponding depths of the present model for this region are shown

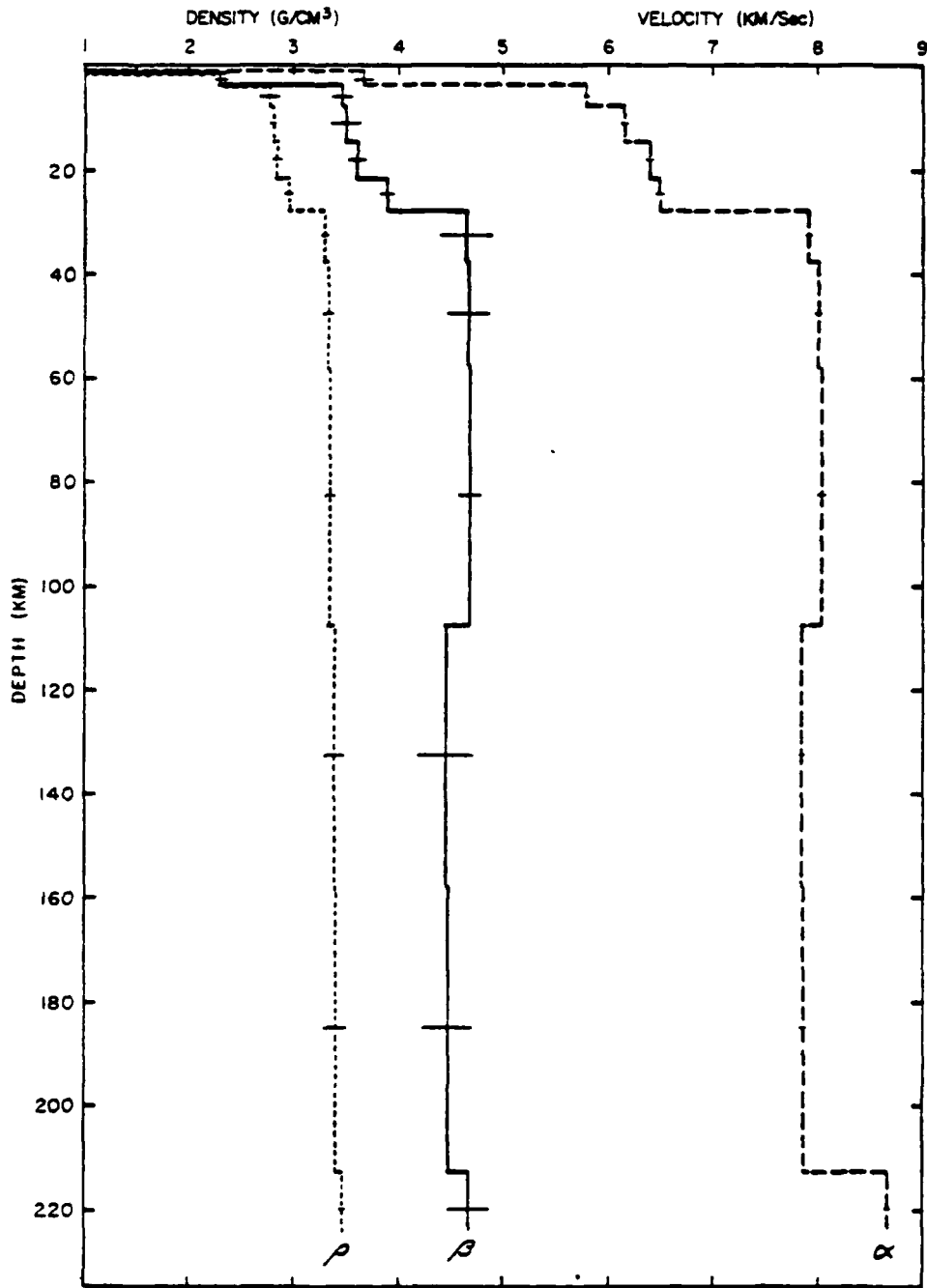


Figure 16: Structure of the Final Model for the Bering Shelf

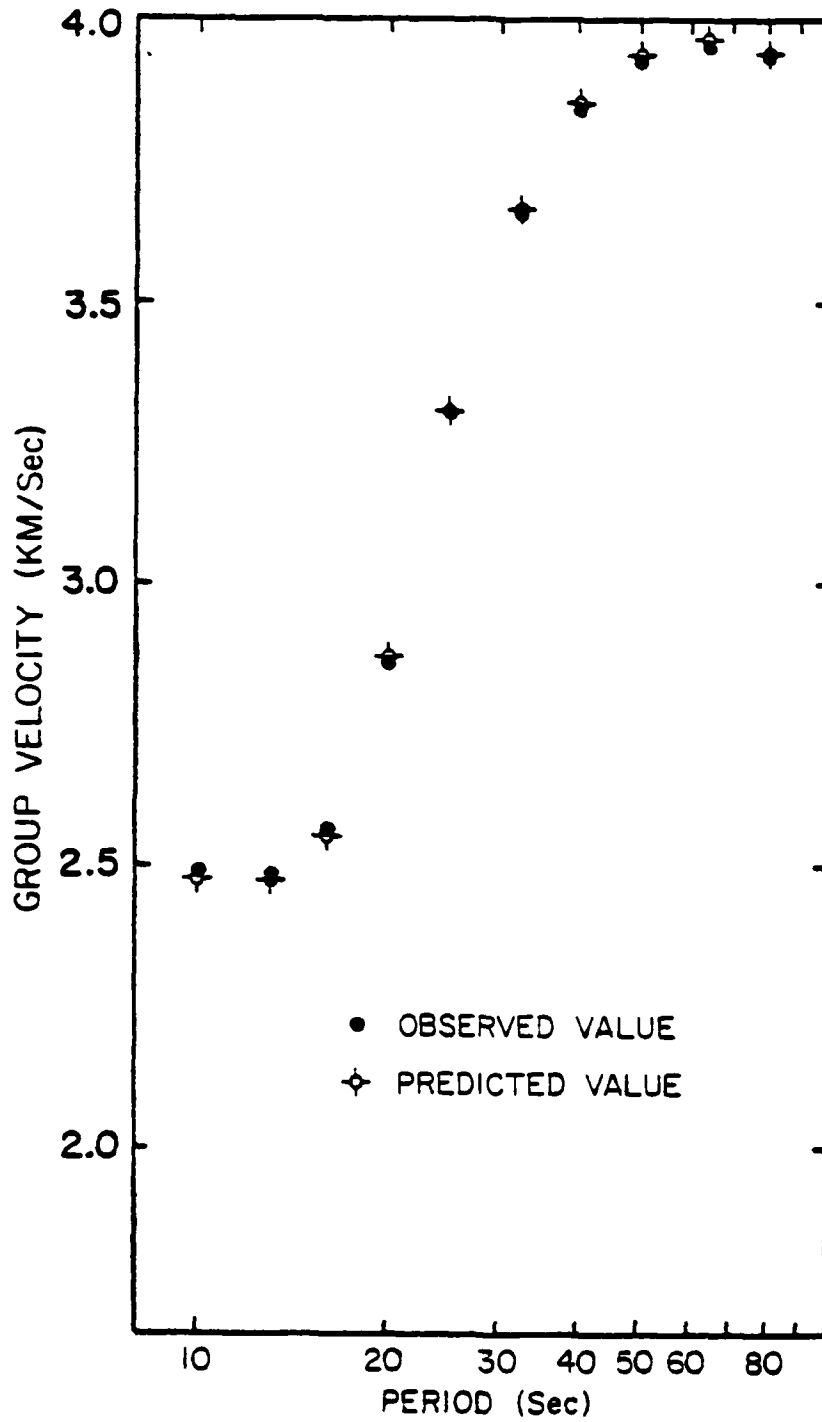


Figure 17: Observed and Predicted Group Velocities for the Bering Shelf

in Figs. 18 and 19, respectively. The weaker resolving power of ρ , and the still weaker resolving power of α which is not shown graphically, compared with that of β are noted from these figures as well as from Figs. 11, 12, 25 and 26. In Fig. 18, the spread is shown for the bottom layer of the crust. The spread is seen to be 14 km. A reasonable estimate for the thickness of the crust for this region is 28 ± 4 km.

The information density of the group velocities used in the inversion process for the Bering Shelf region is shown in Fig. 20. It is seen to have been distorted from the identity matrix to about the same extent as in the continental Alaska region.

3. Aleutian Basin

The initial model for the Aleutian Basin region is shown in Table 7. The group-velocity partial derivatives with respect to the earth parameters for this region are shown for periods 16 and 50 sec in Figs. 21 and 22, respectively. Since the two periods represented in these figures are farther apart than in Figs. 14 and 15 for the Bering Shelf region, the depth shift of the partial-derivative maxima is seen to be more pronounced here than in Figs. 14 and 15. It is also clearly seen from these figures that as the period of waves increases, the shape of the partial derivatives broadens accordingly.

The final model obtained by the analysis of event 2224, with standard deviations of the parameters, is shown in Fig. 23.

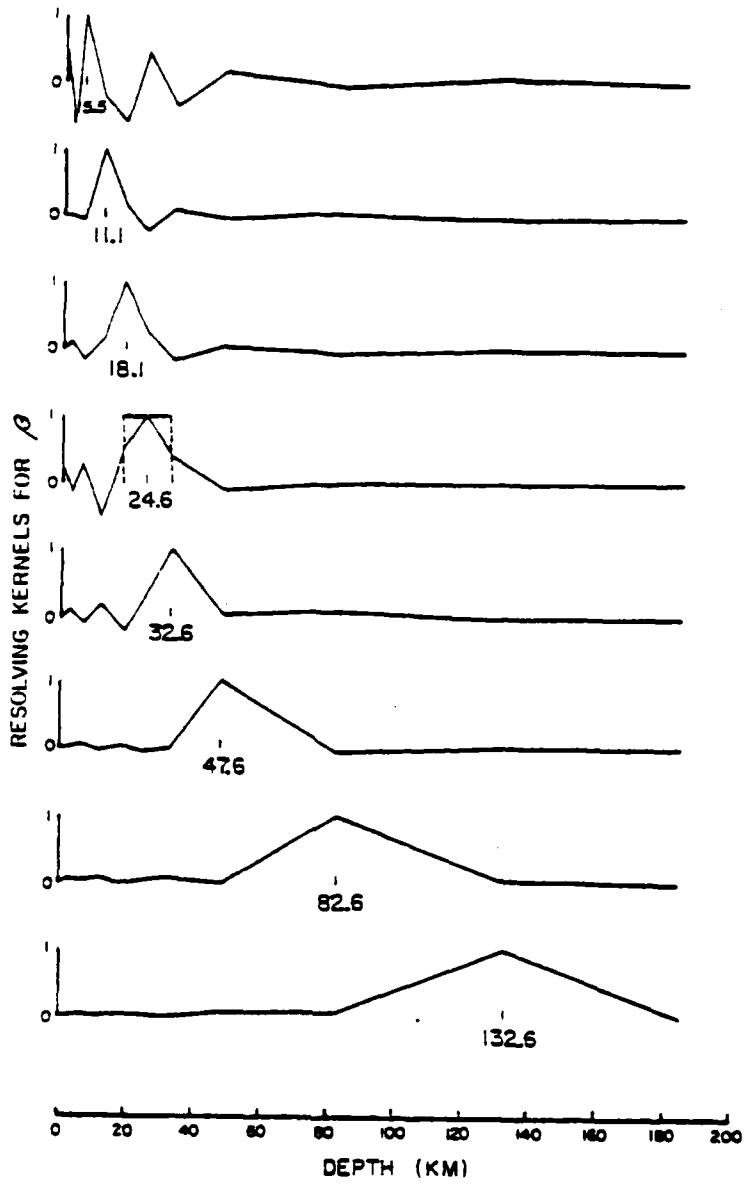


Figure 18: Resolving Kernels for Shear Velocity in the Bering Shelf

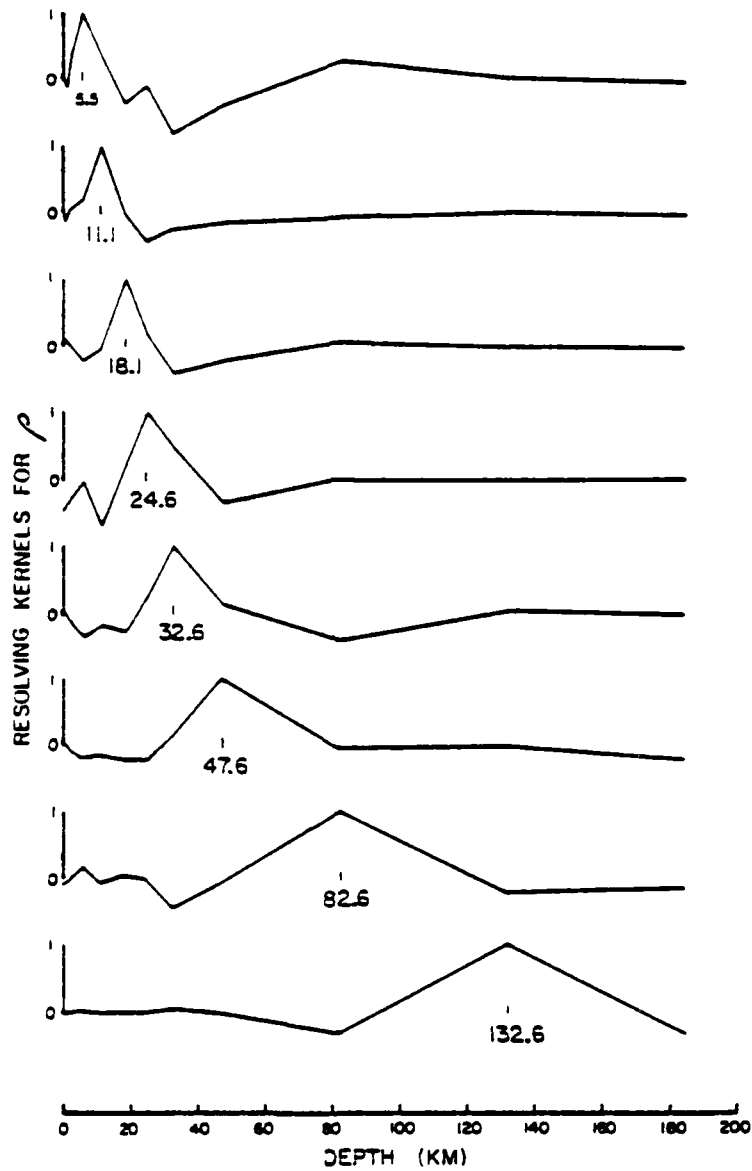


Figure 19: Resolving Kernels for Density in the Bering Shelf

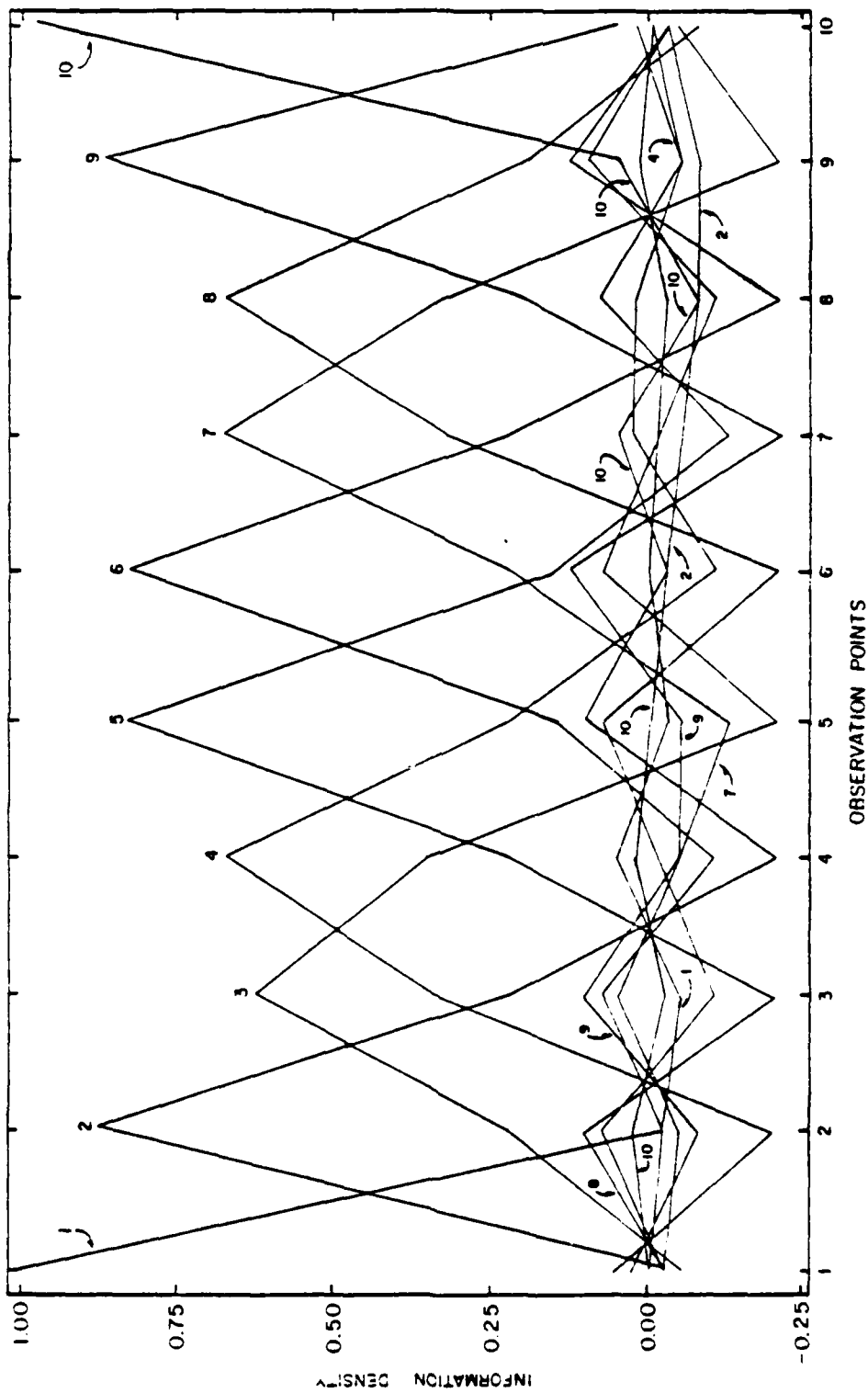


Figure 20: Information Density in the Bering Shelf

TABLE 7
INITIAL MODEL FOR THE ALEUTIAN BASIN

<u>Layer</u>	<u>P-velocity (km/sec)</u>	<u>S-velocity (km/sec)</u>	<u>Density (g/cm³)</u>	<u>Thickness (km)</u>	<u>Depth to Bottom of Layer (km)</u>
0	1.520	0.000	1.030	3.0	3.0
1	2.000	1.000	1.500	1.0	4.0
2	4.556	2.500	2.480	4.8	8.8
3	6.333	3.550	2.867	2.5	11.3
4	7.000	4.000	3.000	6.5	17.8
5	7.900	4.550	3.305	40.0	57.8
6	7.873	4.335	3.359	40.0	97.8
7	7.873	4.335	3.383	40.0	137.8
8	7.873	4.335	3.426	70.0	207.8
9	7.873	4.335	3.432	10.0	217.8
10	8.651	4.652	3.452		

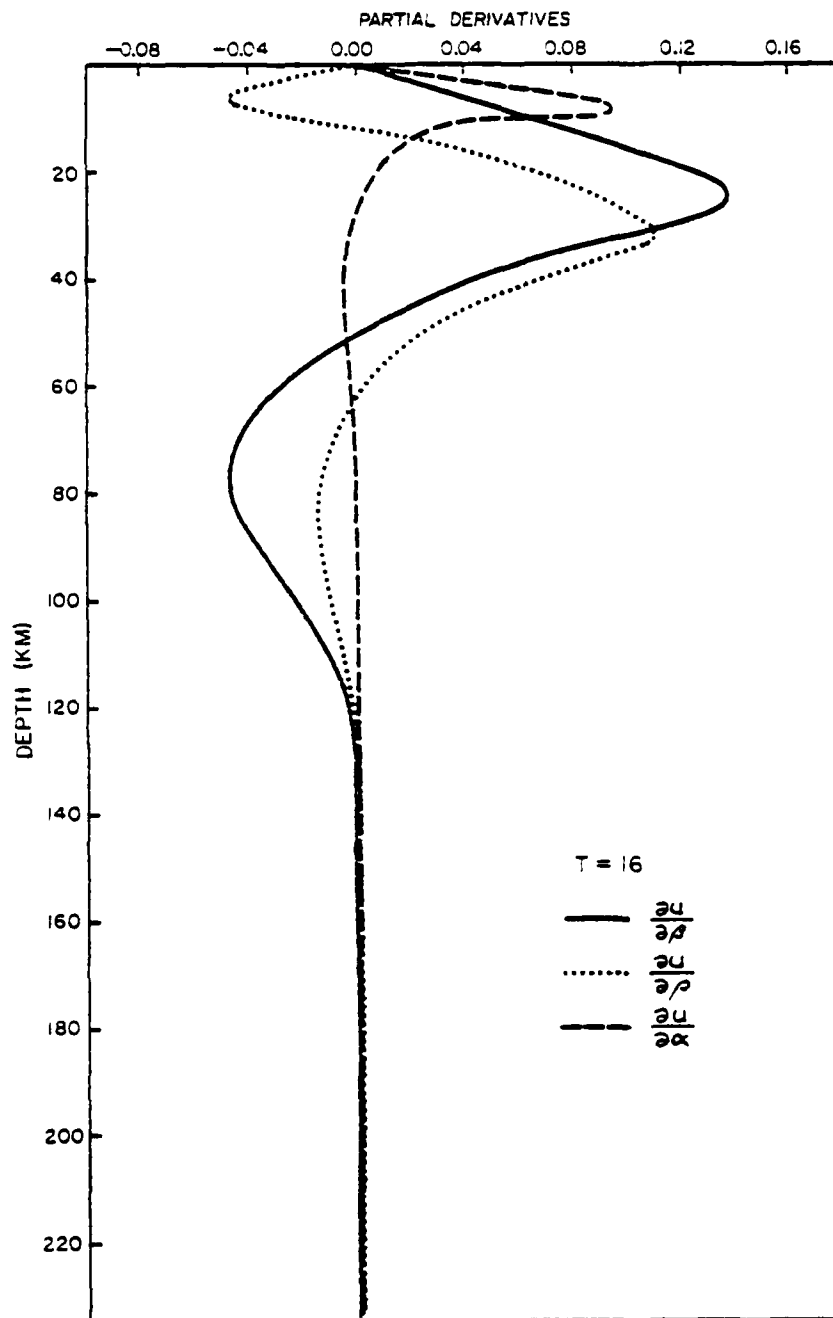


Figure 21: Group Velocity Partial Derivatives for T=16 in the Aleutian Basin

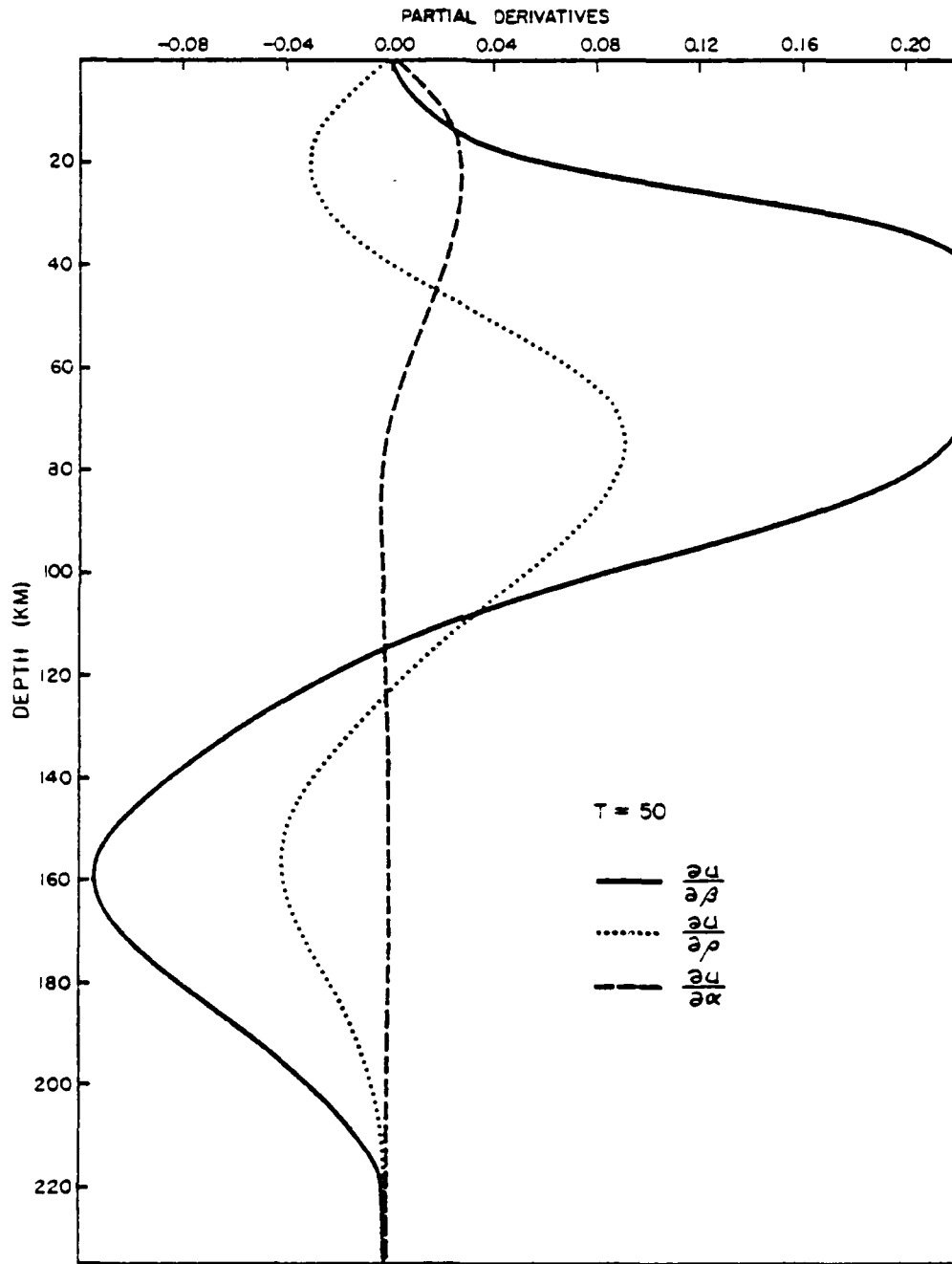


Figure 22: Group Velocity Partial Derivatives for T=50 in the Aleutian Basin

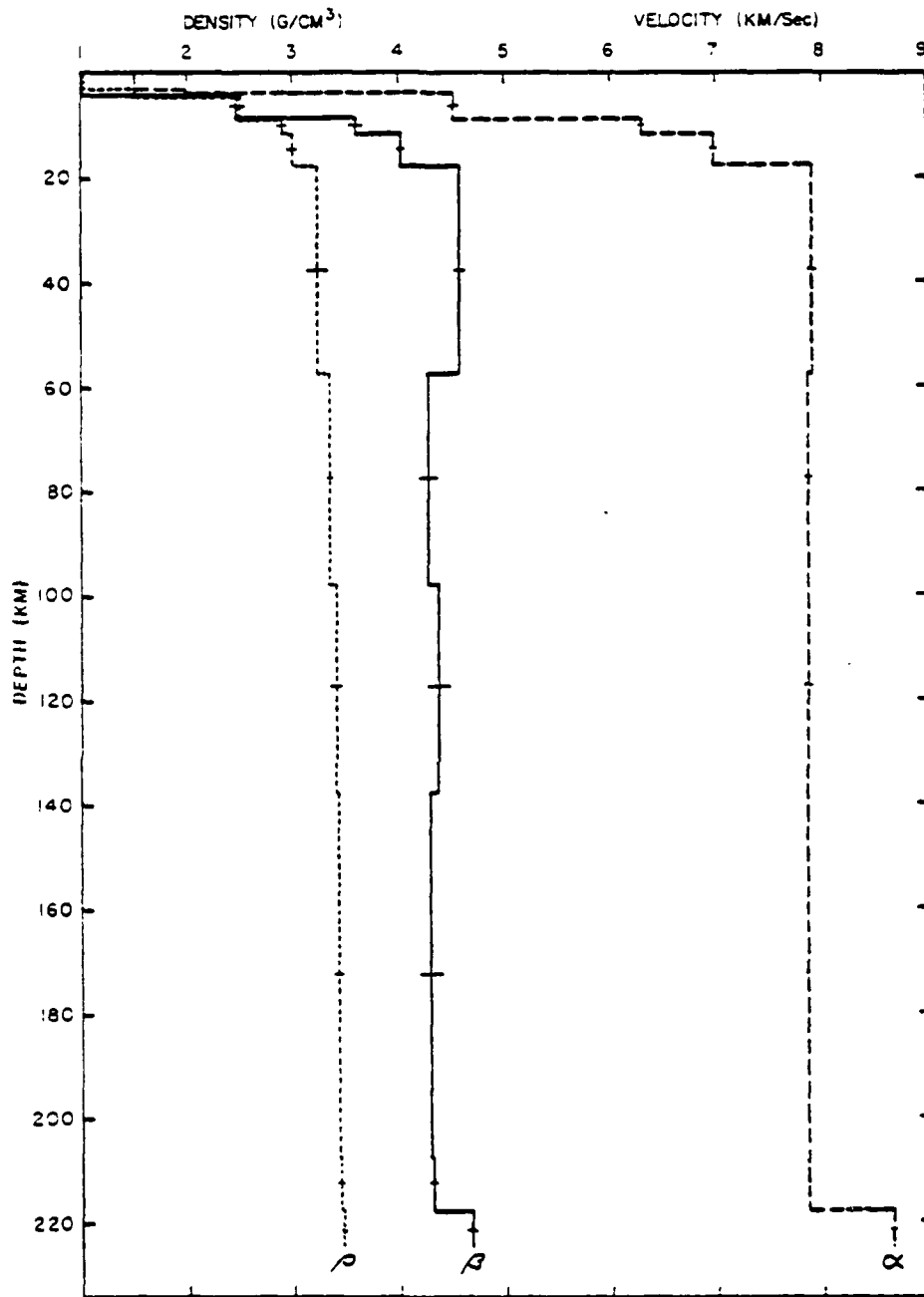


Figure 23: Structure of the Final Model for the Aleutian Basin

The observed and predicted group velocities are shown in Fig. 24. All the differences between the observed and predicted values and their rms error were within the uncertainty of the data. It is found from Fig. 23 that the crustal thickness is 17.8 km. Shor (1964) has estimated the depth to the Moho in this region as 14 km, which was obtained from his refraction analysis. From the results of studies on travel times and waveforms of both refracted and reflected body waves, HelMBERGER (1968) has presented models of the Aleutian Basin. His model with no transition zone between the crust and mantle gives 19 km (his Fig. 10 for station L13) as the depth to the boundary, while his model with one transition layer of thickness less than 1 km shows the depth of the crust-to-mantle transition layer around 16 to 17 km (his Fig. 12).

While HelMBERGER's model with the thick transition zone for his station L9 may be applicable to that part of the Aleutian Basin which is near the Aleutian Islands, the present result of about 18 km may represent the average structure of the Aleutian Basin. It may well be pointed out that the great circle path of event 2224 traverses the middle of the Basin. The crustal structure of the present model is in reasonable agreement with HelMBERGER's model (his Fig. 10).

The present model in Fig. 23 also shows the presence of a LVZ which extends from the depth of about 60 km to about 220 km. The presence and depth range of the present model agree with the parametric oceanic earth model of Dziewonski et al. (1975).

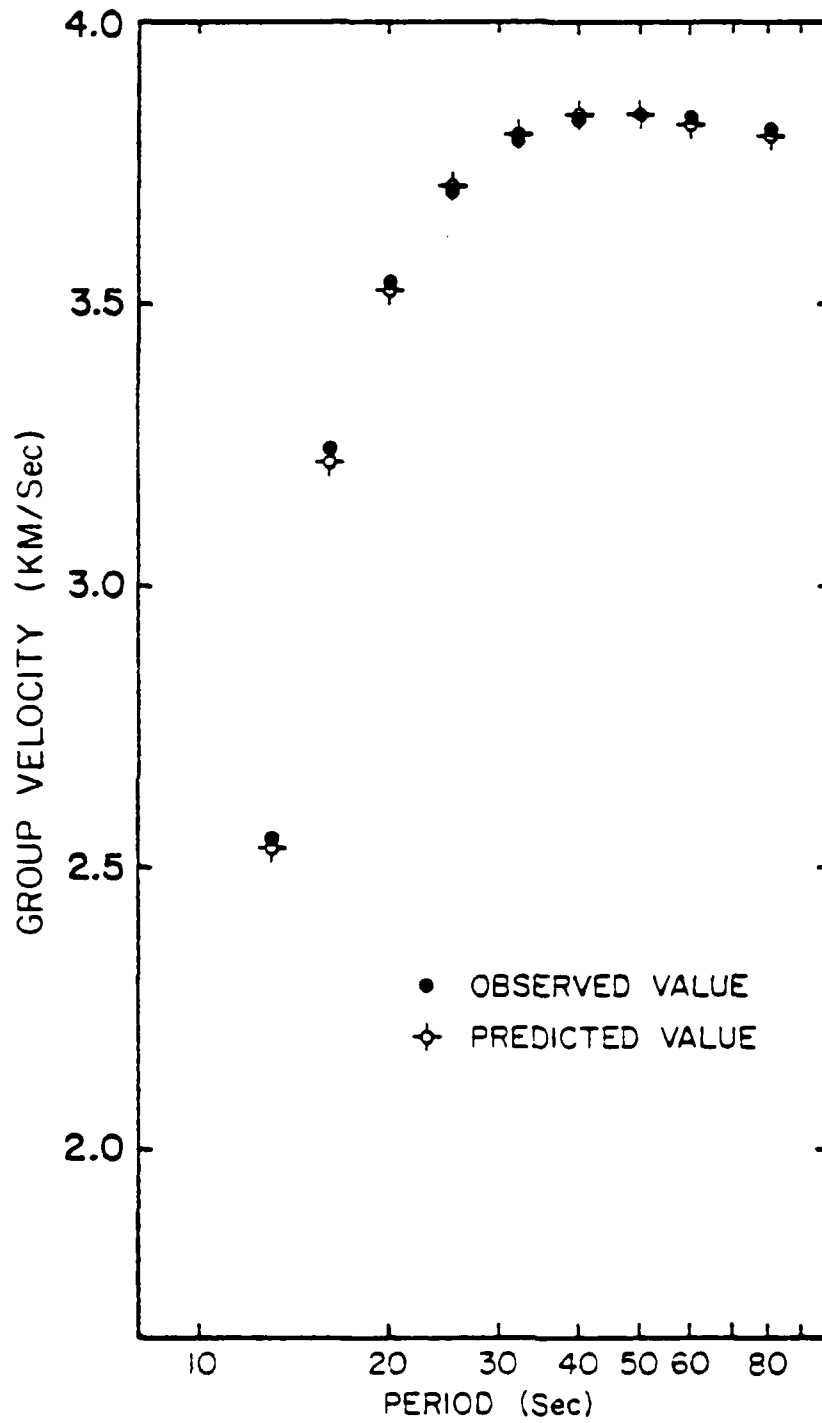


Figure 24: Observed and Predicted Group Velocities for the Aleutian Basin

The resolving kernels of β and ρ of the final model for this region are shown in Figs. 25 and 26, respectively. Depths associated with each kernel are also shown in the figures. The spread for the deepest crustal layer is also shown in connection with the resolving kernel for β of the layer. The spread is 14 km. A reasonable estimate for the crustal thickness of the Aleutian Basin is 18 ± 4 km. Shor's value of 14 km, which is smaller than the present and Helmberger's estimates, may be regarded as a lower limit of the depth to the Moho.

The present result on the structure of the Aleutian Basin shows that, although its crustal thickness is greater than in average oceans, this part of the Bering Sea is oceanic and has not been continentalized in the characteristics of the crust. However, its possibility of conversion from an ocean basin into a continental mass in the future as noted by Shor (1964) remains to be studied.

The information density of the observed group-velocity dispersion relationship used in the inversion for this region is shown in Fig. 27. It is noted from the figure that the information density matrix for this case has been degraded to a greater extent than in cases of continental Alaska and the Bering Shelf. The cause of this greater distortion is thought to be due to the simpler shape of the dispersion curve for this region compared with those of the other regions, while the number of observation periods was the same in all cases.

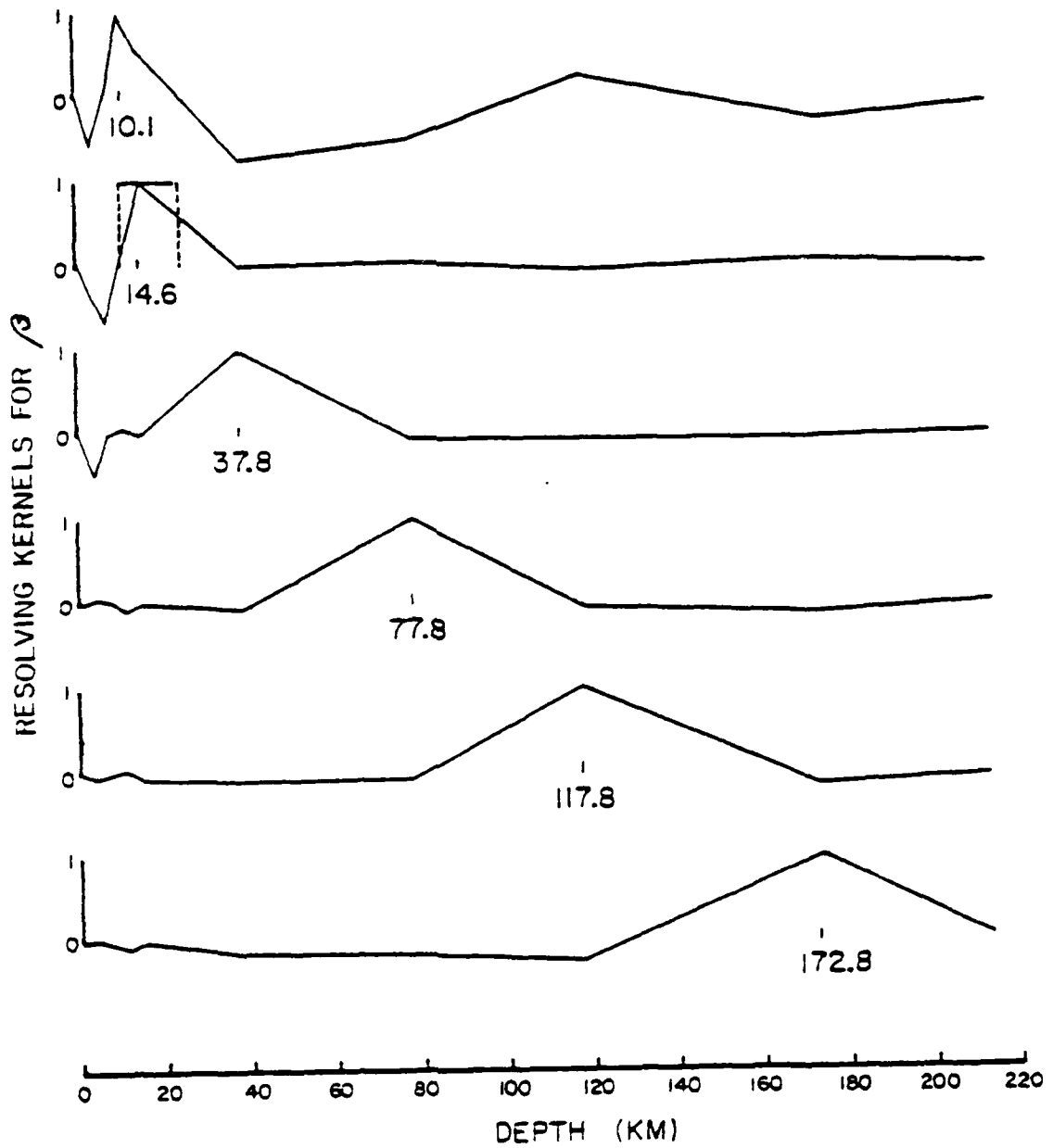


Figure 25: Resolving Kernels for Shear Velocity in the Aleutian Basin

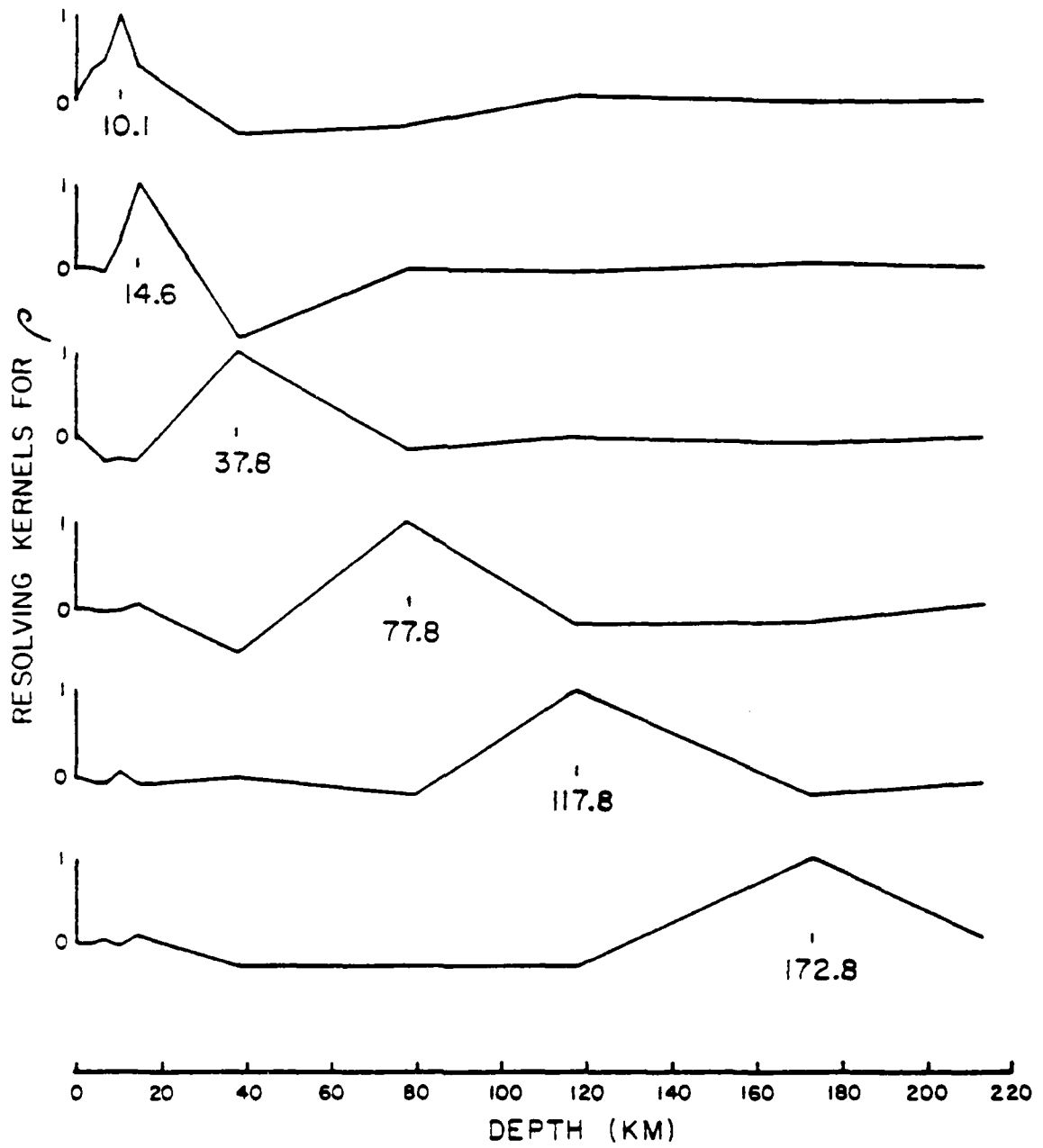


Figure 26: Resolving kernels for density in the Aleutian Basin

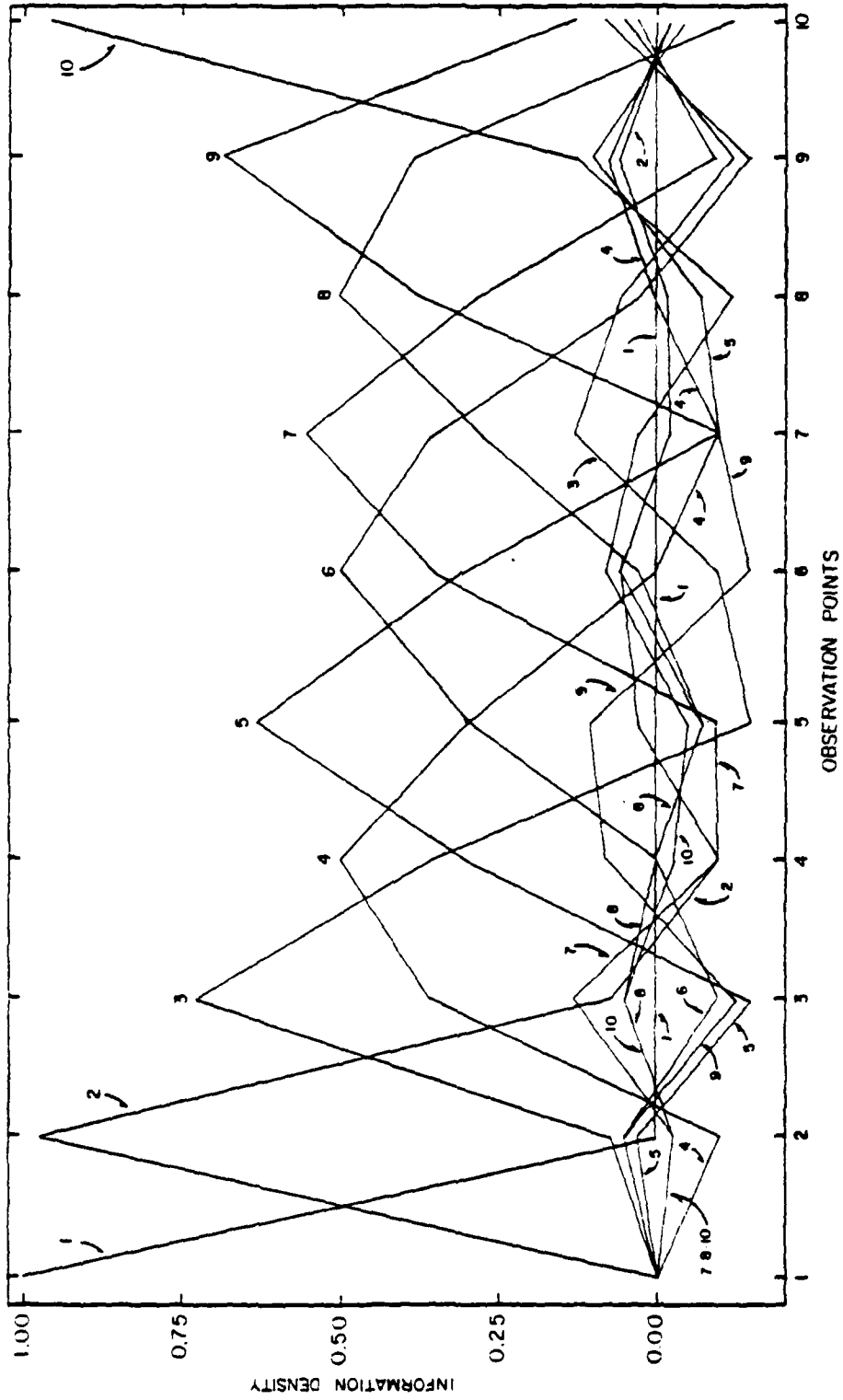


Figure 27: Information Density in the Aleutian Basin

Thus we have obtained estimates of the structure of the three provinces of the study area. In order to utilize the additional data available, the observations from the events 1519 and 2005, and to check the results obtained above, the following efforts were made. From the experience gained to this point, the author has learned that it took many trials and accompanying time of considerable amount to find a "good" initial model which gives a satisfactory convergence of predicted data to the observed one. Therefore instead of repeating the inversion procedures with the rest of the observed data, it was decided to solve a forward problem with the structures obtained and with appropriate proportions of path length and to compare the results with observed data.

With the information as shown in Figs. 9, 16 and 23, and Table 2, group velocities were calculated for events 1519 and 2005 and the results along with the observed group velocities are shown in Figs. 28 and 29. As can be seen from the figures, the agreement between the observed and predicted values was very good except at a few of the shortest periods. These results are therefore in agreement with the final models we have obtained.

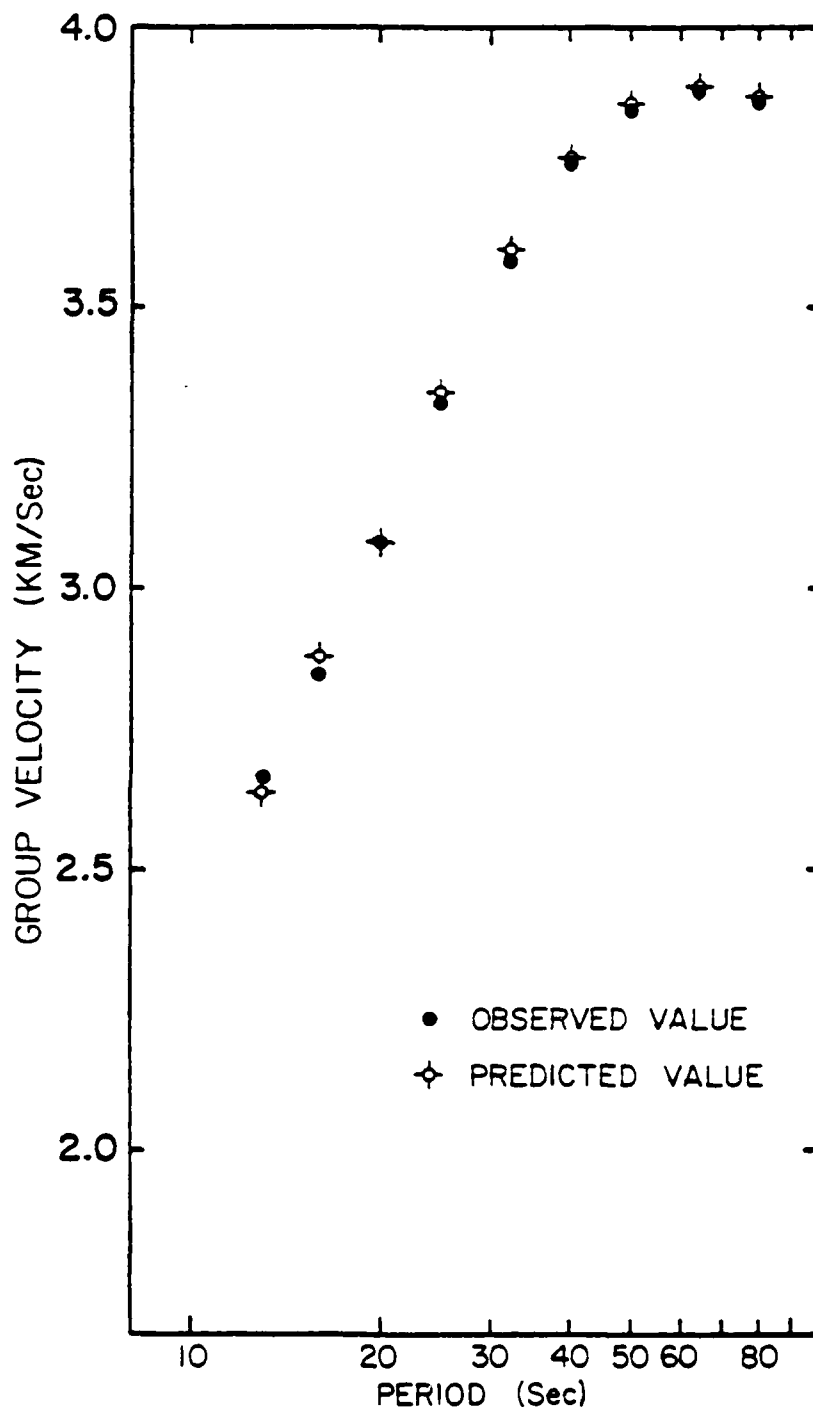


Figure 28: Observed and Predicted Group Velocities for Event 1519

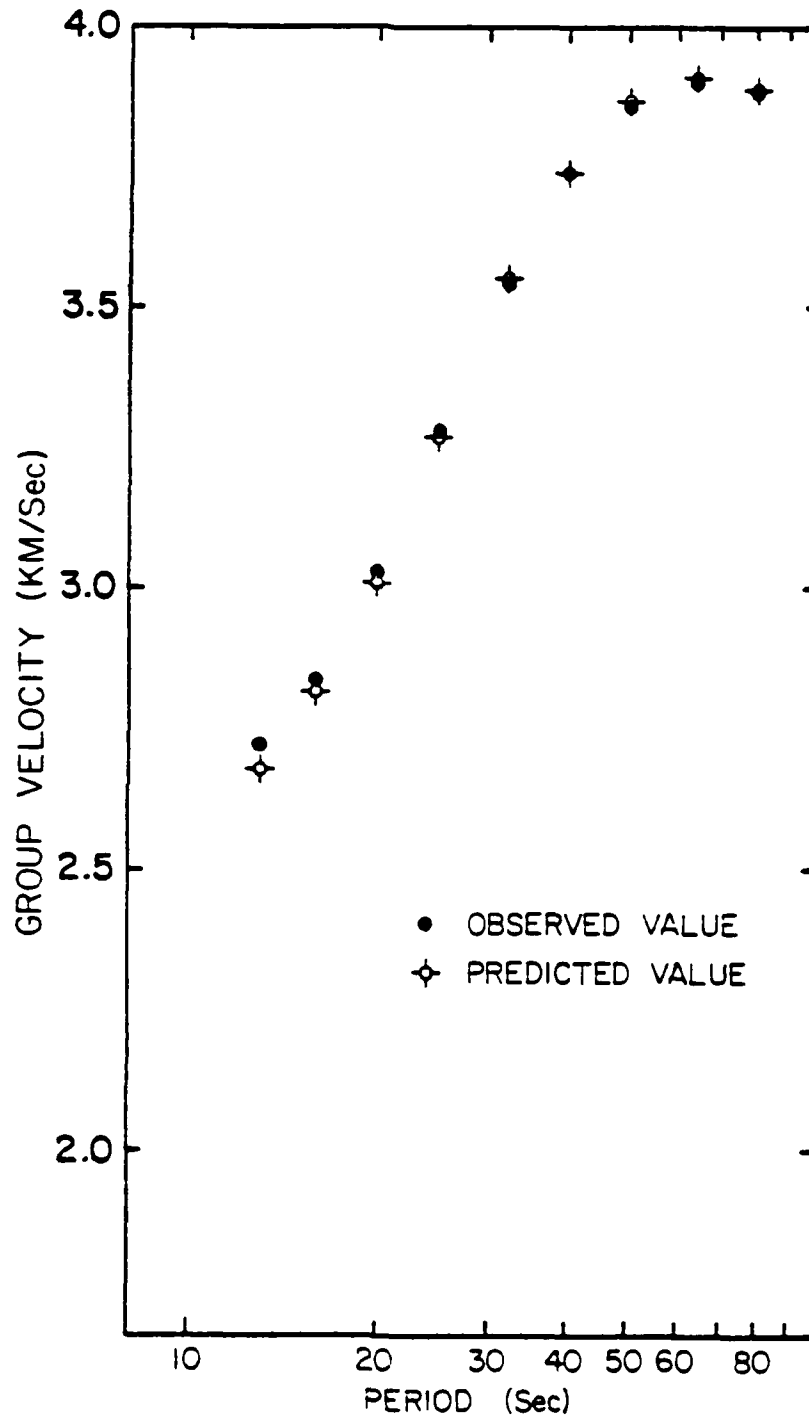


Figure 29: Observed and Predicted Group Velocities for Event 2005

CONCLUSION

From the studies of surface waves by the method described in this study and the results discussed in the last chapter, the following conclusions are drawn:

1. Phase-matched filtering has been effective in determining group-velocity dispersion curves in the present study area. The curves have been inverted and checked with previous results of gravitational, seismic refraction and reflection studies.
2. The best estimates of the group-velocity dispersion relationships in the area studied have been obtained and presented in Fig. 5.
3. The great circle paths for the events used in this study appear to coincide with the least-time paths. This was the case due to the geometric arrangements of the physiographic provinces and their boundaries of the study area relative to the source-station pairs.
4. The method of studying a compound area by dividing it into two or more "pure-path" provinces proved effective under the circumstances described in the last sentence. The group-velocity dispersion relationships derived from this method for the "pure-path" provinces of the Bering Shelf and the Aleutian Basin are presented in Figs. 17 and 24, respectively.

5. The exact analytical method formulated in this study for the computation of Rayleigh-wave phase-velocity partial derivatives with respect to earth parameters has proved effective, has not shown any numerical difficulties when coded with double precision, and has been successfully incorporated into a generalized linear inversion algorithm.

6. A generalized linear inversion method has been applied to an inversion of group-velocity dispersion relationships in order to find the shear-wave velocity, density and compressional-wave velocity structure of the earth. The results have yielded the following estimates:

(i) The average crustal thickness of the continental Alaska region studied is 43 ± 3 km. A LVZ is present in this region and extends from about 113 to about 213 km depth.

(ii) The depth to the Moho in the Bering Shelf region is 28 ± 4 km. A LVZ ranges in depth from about 108 to about 213 km.

(iii) The crust in the Aleutian Basin region is oceanic in nature and the boundary between the continental Bering Shelf and the oceanic Aleutian Basin appears to lie near and parallel to the 1000-fathom bathymetric contour line.

(iv) The thickness of the crust in the Aleutian Basin region is 18 ± 4 km. A LVZ is present in this region and extends from about 60 to about 220 km depth.

APPENDIX

Expressions necessary to compute the phase-velocity partial derivatives are given below. It is hoped that these expressions, although somewhat lengthy, will give those who use the method of this paper a convenience and saving of time required to carry through the very time-consuming and tedious calculations. It should be noted that in the case of Rayleigh waves, there are three situations in connection with the relation between the phase velocity and body-wave velocities. They are: (1) $c > \alpha_m$ and $c > \beta_m$, i.e., both \mathcal{N}_{α_m} and \mathcal{N}_{β_m} are positive real; (2) $c < \alpha_m$ and $c > \beta_m$, i.e., \mathcal{N}_{α_m} is negative pure imaginary while \mathcal{N}_{β_m} is positive real; (3) $c < \alpha_m$ and $c < \beta_m$, i.e., both \mathcal{N}_{α_m} and \mathcal{N}_{β_m} are negative pure imaginary. In the following expressions a triple sign--three signs put together vertically--applies, in the order from top to bottom, to the above three cases. When the three cases have a common sign, only a single sign appears. It is also understood that whenever \mathcal{N}_{α_m} and \mathcal{N}_{β_m} are pure imaginary, \mathcal{N}_{α_m} and \mathcal{N}_{β_m} in the following expressions actually represent $\mathcal{N}_{\alpha_m}^*$ and $\mathcal{N}_{\beta_m}^*$, respectively; and trigonometric functions become corresponding hyperbolic functions.

Since the elements of the layer matrix have been published previously, see Haskell (1953, p. 21) and Harkrider (1964, Eq. 16), only their partial derivatives are presented here.

$$\frac{\partial (a_m)_{11}}{\partial \alpha_m} = \frac{-}{+} \frac{c \omega d_m \gamma_m \sin P_m}{\alpha_m^3 \mathcal{R}_{\alpha m}}$$

$$\frac{\partial (a_m)_{11}}{\partial \beta_m} = \frac{4\beta_m}{c^2} (\cos P_m - \cos Q_m) - \frac{c \omega d_m (\gamma_m - 1) \sin Q_m}{\beta_m^3 \mathcal{R}_{\beta m}}$$

$$\frac{\partial (a_m)_{11}}{\partial P_m} = 0$$

$$\frac{\partial (a_m)_{11}}{\partial d_m} = k \left[\frac{-}{+} \gamma_m \mathcal{R}_{\alpha m} \sin P_m \pm (\gamma_m - 1) \mathcal{R}_{\beta m} \sin Q_m \right]$$

$$\frac{\partial (a_m)_{11}}{\partial c} = -\frac{1}{c} \left[2\gamma_m (\cos P_m - \cos Q_m) + \frac{1}{\mathcal{R}_{\alpha m} \mathcal{R}_{\beta m}} \{ \gamma_m Q_m \sin P_m - (\gamma_m - 1) P_m \sin Q_m \} \right]$$

$$\frac{\partial (a_m)_{12}}{\partial \alpha_m} = \frac{-}{+} i \frac{c^2 (\gamma_m - 1)}{\alpha_m^3 \mathcal{R}_{\alpha m}} (P_m \cos P_m - \sin P_m)$$

$$\frac{\partial (a_m)_{12}}{\partial \beta_m} = 2i \left[\frac{2\beta_m}{c^2} \left(\frac{\sin P_m}{\mathcal{R}_{\alpha m}} \pm \mathcal{R}_{\beta m} \sin Q_m \right) - \frac{1}{\beta_m \mathcal{R}_{\beta m}} (\sin Q_m + Q_m \cos Q_m) \right]$$

$$\frac{\partial (a_m)_{12}}{\partial P_m} = 0$$

$$\frac{\partial (a_m)_{12}}{\partial d_m} = i k \left[(\gamma_m - 1) \cos P_m \pm \gamma_m \mathcal{R}_{\beta m}^2 \cos Q_m \right]$$

$$\frac{\partial (a_m)_{12}}{\partial c} = \frac{i}{c} \left[\frac{\gamma_m - 1}{\mathcal{R}_{\alpha m} (c^2 - d_m^2)} (\alpha_m^2 P_m \cos P_m \mp c^2 \sin P_m) \right.$$

$$\left. + \gamma_m \left(k d_m \cos Q_m \mp 2 \mathcal{R}_{\beta m} \sin Q_m + \frac{c^2 \sin Q_m}{\beta_m^2 \mathcal{R}_{\beta m}} - \frac{2 \sin P_m}{\mathcal{R}_{\alpha m}} \right) \right]$$

$$\frac{\partial (a_m)_{13}}{\partial \alpha_m} = -\frac{k d_m \sin P_m}{P_m \alpha_m^3 \mathcal{R}_{\alpha m}}$$

$$\frac{\partial (A_m)_{13}}{\partial \beta_m} = \frac{k d_m \sin Q_m}{\rho_m \beta_m^3 \rho_{\beta m}}$$

$$\frac{\partial (A_m)_{13}}{\partial \rho_m} = \frac{1}{c^2 \rho_m^2} (\cos P_m - \cos Q_m)$$

$$\frac{\partial (A_m)_{13}}{\partial d_m} = \frac{k}{c^2 \rho_m} \left(\frac{+}{-} \rho_{\alpha m} \sin P_m \mp \rho_{\beta m} \sin Q_m \right)$$

$$\frac{\partial (A_m)_{13}}{\partial c} = \frac{1}{c^3 \rho_m} \left[2 (\cos P_m - \cos Q_m) + \frac{1}{\rho_{\alpha m} \rho_{\beta m}} (Q_m \sin P_m - P_m \sin Q_m) \right]$$

$$\frac{\partial (A_m)_{14}}{\partial d_m} = \mp \frac{i}{\rho_m \alpha_m^3 \rho_{\alpha m}} (P_m \cos P_m - \sin P_m)$$

$$\frac{\partial (A_m)_{14}}{\partial \beta_m} = - \frac{i}{\rho_m \beta_m^3 \rho_{\beta m}} (\sin Q_m + Q_m \cos Q_m)$$

$$\frac{\partial (A_m)_{14}}{\partial \rho_m} = - \frac{i}{c^2 \rho_m^2} \left(\frac{\sin P_m}{\rho_{\alpha m}} \mp \rho_{\beta m} \sin Q_m \right)$$

$$\frac{\partial (A_m)_{14}}{\partial d_m} = i \frac{k}{c^2 \rho_m} (\cos P_m \mp \rho_{\beta m}^2 \cos Q_m)$$

$$\frac{\partial (A_m)_{14}}{\partial c} = - \frac{i}{c^3 \rho_m} \left[2 \left(\frac{\sin P_m}{\rho_{\alpha m}} \mp \rho_{\beta m} \sin Q_m \right) \mp \frac{1}{\rho_{\alpha m}^3} (P_m \cos P_m - \frac{c^2 \sin P_m}{\alpha_m^2}) \right.$$

$$\left. - \frac{c^2 \sin Q_m}{\beta_m^2 \rho_{\beta m}} - k d_m \cos Q_m \right]$$

$$\frac{\partial (A_m)_{21}}{\partial d_m} = i \frac{2 \beta_m^2}{\alpha_m^3 \rho_{\alpha m}} (\sin P_m + P_m \cos P_m)$$

$$\frac{\partial (A_m)_{21}}{\partial \beta_m} = -i \left[\frac{4 \beta_m}{c^2} \left(\frac{\sin Q_m}{\rho_{\beta m}} \mp \rho_{\alpha m} \sin P_m \right) \mp \frac{c^2 (\delta_m - 1)}{\beta_m^3 \rho_{\beta m}} (\sin Q_m - Q_m \cos Q_m) \right]$$

$$\frac{\partial (a_m)_{21}}{\partial \beta_m} = 0$$

$$\frac{\partial (a_m)_{21}}{\partial d_m} = -ik \left[(\gamma_m - 1) \cos Q_m \mp \gamma_m \alpha_m^2 \cos P_m \right]$$

$$\begin{aligned} \frac{\partial (a_m)_{21}}{\partial c} = & -i \left[\gamma_m \left\{ \frac{1}{c} (k d_m \cos P_m \mp 2 \alpha_m \sin P_m) + \frac{c \sin P_m}{\alpha_m^2 \alpha_m} \right\} - \frac{2 \gamma_m \sin Q_m}{c \alpha_m} \right. \\ & \left. \mp \frac{\gamma_m - 1}{\alpha_m^3} \left(\frac{\alpha_m \cos Q_m}{c} - \frac{c \sin Q_m}{\beta_m^2} \right) \right] \end{aligned}$$

$$\frac{\partial (a_m)_{22}}{\partial d_m} = - \frac{c^2 k d_m (\gamma_m - 1) \sin P_m}{\alpha_m^3 \alpha_m}$$

$$\frac{\partial (a_m)_{22}}{\partial \beta_m} = \frac{4 \beta_m}{c^2} (\cos Q_m - \cos P_m) + \frac{2 k d_m \sin Q_m}{\beta_m \alpha_m}$$

$$\frac{\partial (a_m)_{22}}{\partial \beta_m} = 0$$

$$\frac{\partial (a_m)_{22}}{\partial d_m} = k \left[\frac{+}{-} (\gamma_m - 1) \alpha_m \sin P_m \mp \gamma_m \alpha_m \sin Q_m \right]$$

$$\frac{\partial (a_m)_{22}}{\partial c} = \frac{1}{c} \left[2 \gamma_m (\cos P_m - \cos Q_m) + \frac{1}{\alpha_m \beta_m} \{ (\gamma_m - 1) \alpha_m \sin P_m - \gamma_m \beta_m \sin Q_m \} \right]$$

$$\frac{\partial (a_m)_{23}}{\partial d_m} = - \frac{i}{\beta_m \alpha_m^3 \alpha_m} (\sin P_m + \beta_m \cos P_m)$$

$$\frac{\partial (a_m)_{23}}{\partial \beta_m} = \frac{i}{\beta_m \beta_m^3 \alpha_m} (\alpha_m \cos Q_m - \sin Q_m)$$

$$\frac{\partial (a_m)_{23}}{\partial \beta_m} = \frac{i}{c^2 \beta_m^2} \left(\frac{-}{+} \alpha_m \sin P_m - \frac{\sin Q_m}{\alpha_m} \right)$$

$$\frac{\partial (a_m)_{23}}{\partial d_m} = i \frac{k}{c^2 \rho_m} \left(\frac{+}{-} \rho_{dm}^2 \cos P_m + \cos Q_m \right)$$

$$\begin{aligned} \frac{\partial (a_m)_{23}}{\partial c} &= -\frac{i}{c^3 \rho_m} \left[2 \left(\frac{\sin Q_m}{\rho_{\beta m}} \frac{+}{-} \rho_{dm} \sin P_m \right) - k d_m \cos P_m - \frac{c^2 \sin P_m}{\alpha_m^2 \rho_{dm}} \right. \\ &\quad \left. - \frac{1}{\rho_{\beta m}^2} \left(Q_m \cos Q_m - \frac{c^2 \sin Q_m}{\beta_m^2} \right) \right] \end{aligned}$$

$$\frac{\partial (a_m)_{31}}{\partial d_m} = \frac{c^4 \rho_m k d_m \gamma_m (\gamma_m - 1) \sin P_m}{\alpha_m^3 \rho_{dm}}$$

$$\frac{\partial (a_m)_{31}}{\partial \beta_m} = 2 \rho_m \left[2 \beta_m (2 \gamma_m - 1) (\cos P_m - \cos Q_m) - \frac{c^2 (\gamma_m - 1) k d_m \sin Q_m}{\beta_m \rho_{\beta m}} \right]$$

$$\frac{\partial (a_m)_{31}}{\partial \rho_m} = 2 \beta_m^2 (\gamma_m - 1) (\cos P_m - \cos Q_m)$$

$$\frac{\partial (a_m)_{31}}{\partial d_m} = 2 k \rho_m \beta_m^2 (\gamma_m - 1) \left(\frac{+}{-} \rho_{dm} \sin P_m \frac{+}{-} \rho_{\beta m} \sin Q_m \right)$$

$$\frac{\partial (a_m)_{31}}{\partial c} = c \rho_m \gamma_m \left[2 \gamma_m (\cos Q_m - \cos P_m) + \frac{\gamma_m - 1}{\rho_{dm} \rho_{\beta m}} (P_m \sin Q_m - Q_m \sin P_m) \right]$$

$$\frac{\partial (a_m)_{32}}{\partial d_m} = \frac{+}{-} i \frac{c^4 \rho_m (\gamma_m - 1)^2}{\alpha_m^3 \rho_{dm}^3} (\sin P_m - P_m \cos P_m)$$

$$\frac{\partial (a_m)_{32}}{\partial \beta_m} = i 4 \rho_m \beta_m \left[2 \left\{ \frac{(\gamma_m - 1) \sin P_m}{\rho_{dm}} \frac{+}{-} \gamma_m \rho_{\beta m} \sin Q_m \right\} - \frac{1}{\rho_{\beta m}} (\sin Q_m + Q_m \cos Q_m) \right]$$

$$\frac{\partial (a_m)_{32}}{\partial \rho_m} = i c^2 \left[\frac{(\gamma_m - 1)^2 \sin P_m}{\rho_{dm}} \frac{+}{-} \gamma_m^2 \rho_{\beta m} \sin Q_m \right]$$

$$\frac{\partial (a_m)_{32}}{\partial d_m} = i k c^2 \rho_m \left[(\gamma_m - 1)^2 \cos P_m \frac{+}{-} \gamma_m^2 \rho_{\beta m}^2 \cos Q_m \right]$$

$$\frac{\partial (a_m)_{32}}{\partial c} = -i \rho_m \left[\frac{c}{R_{dm}} \left\{ 2(\gamma_m^2 - 1) \sin P_m \mp \frac{(\gamma_m - 1)^2}{R_{dm}^2} (P_m \cos P_m - \frac{c^2 \sin P_m}{\alpha_m^2}) \right\} \right. \\ \left. \mp \frac{4\beta_m^2}{c} (\gamma_m R_{\beta m} \sin Q_m \mp \frac{\sin Q_m}{R_{\beta m}}) - \omega d_m \gamma_m^2 \cos Q_m \right]$$

$$\frac{\partial (a_m)_{41}}{\partial d_m} = -i \frac{4\rho_m \beta_m^4}{\alpha_m^2 R_{dm}} (\sin P_m + P_m \cos P_m)$$

$$\frac{\partial (a_m)_{41}}{\partial \beta_m} = i c^2 \rho_m \left[\frac{8\beta_m}{c^2} \left\{ \frac{(\gamma_m - 1) \sin Q_m}{R_{\beta m}} \mp \gamma_m R_{dm} \sin P_m \right\} \right. \\ \left. \mp \frac{c^2 (\gamma_m - 1)^2}{\beta_m^2 R_{\beta m}} (\sin Q_m - Q_m \cos Q_m) \right]$$

$$\frac{\partial (a_m)_{41}}{\partial \rho_m} = i c^2 \left[\frac{(\gamma_m - 1)^2 \sin Q_m}{R_{\beta m}} \mp \gamma_m^2 R_{dm} \sin P_m \right]$$

$$\frac{\partial (a_m)_{41}}{\partial d_m} = i k c^2 \rho_m \left[(\gamma_m - 1)^2 \cos Q_m \mp \gamma_m^2 R_{dm}^2 \cos P_m \right]$$

$$\frac{\partial (a_m)_{41}}{\partial c} = i \rho_m \left[\omega d_m \gamma_m^2 \cos P_m \mp \frac{4\beta_m^2}{c} (\gamma_m R_{dm} \sin P_m \mp \frac{\beta_m^2 \sin P_m}{\alpha_m^2 R_{dm}}) \right. \\ \left. - \frac{c}{R_{\beta m}} \left\{ 2(\gamma_m^2 - 1) \sin Q_m \mp \frac{(\gamma_m - 1)^2}{R_{\beta m}^2} (Q_m \cos Q_m - \frac{c^2 \sin Q_m}{\beta_m^2}) \right\} \right]$$

$$(a_m)_{24} = (a_m)_{13}; \quad (a_m)_{33} = (a_m)_{22}; \quad (a_m)_{34} = (a_m)_{12}; \quad (a_m)_{42} = (a_m)_{31};$$

$$(a_m)_{43} = (a_m)_{21}; \quad (a_m)_{44} = (a_m)_{11};$$

$$\frac{\partial T^*}{\partial c} = \frac{\rho_0}{c^2 - \alpha_0^2} \left[\omega d_0 \alpha_0^2 \sec^2 P_0 + \frac{c(c^2 - 2\alpha_0^2) \tan P_0}{R_{\alpha 0}} \right].$$

BIBLIOGRAPHY

- Anderson, D.L., 1964. Universal dispersion tables I. Love waves across oceans and continents on a spherical earth, Bull. Seism. Soc. Am., 54, 681-726.
- Anderson, D.L. and Harkrider, D.G., 1968. Universal dispersion tables II. Variational parameters for amplitudes, phase velocity and group velocity for first four Love modes for an oceanic and a continental earth model, Bull. Seism. Soc. Am., 58, 1407-1499.
- Backus, G.E. and Gilbert, J.F., 1967. Numerical applications of a formalism for geophysical inverse problems, Geophys. J., 13, 247-276.
- Backus, G. and Gilbert, F., 1968. The resolving power of gross earth data, Geophys. J., 16, 169-205.
- Backus, G. and Gilbert F., 1970. Uniqueness in the inversion of inaccurate gross earth data, Phil. Trans. Roy. Soc. London, Ser. A., 266, 123-192.
- Bendat, J.S., 1958. Principles and applications of random noise theory, John Wiley and Sons, New York, 431 pp.
- Biswas, N.N. and Knopoff, L., 1970. An exact earth flattening correction for Love waves, Bull. Seism. Soc. Am., 60, 1123-1127.

- Bloch, S., Hales, A.L., and Landisman, M., 1969. Velocities in the crust and upper mantle of southern Africa from multi-mode surface wave dispersion, Bull. Seism. Soc. Am., 59, 1599-1629.
- Bolt, B.A. and Dorman, J., 1961. Phase and group velocities of Rayleigh waves in a spherical, gravitating earth, J. Geophys. Res., 66, 2965-2981.
- Braile, L.W. and Keller, G.R., 1975. Fine structure of the crust inferred from linear inversion of Rayleigh-wave dispersion, Bull. Seism. Soc. Am., 65, 71-83.
- Braile, L.W., Keller, G.R., and Peeples, W.J., 1974. Inversion of gravity data for two-dimensional density distributions, J. Geophys. Res., 79, 2017-2021.
- Brune, J. and Dorman, J., 1963. Seismic waves and earth structure in the Canadian Shield, Bull. Seism. Soc. Am., 53, 167-210.
- Der, Z.A. and Landisman, M., 1972. Theory for errors, resolution and separation of unknown variables in inverse problems, with application to the mantle and the crust in southern Africa and Scandinavia, Geophys. J., 27, 137-178.
- Der, Z., Masse, R., and Landisman, M., 1970. Effects of observational errors on the resolution of surface waves at intermediate distances, J. Geophys. Res., 75, 3399-3409.

- Dorman, J. and Ewing, M., 1962. Numerical inversion of seismic surface wave dispersion data and crust-mantle structure in the New York-Pennsylvania area, J. Geophys. Res., 67, 5227-5241.
- Dziewonski, A., Bloch, S., and Landisman, M., 1969. A technique for the analysis of transient seismic signals, Bull. Seism. Soc. Am., 59, 427-444.
- Dziewonski, A.M., Hales, A.L., and Lapwood, E.R., 1975, Parametrically simple earth models consistent with geophysical data, Phys. Earth Plan. Int., 10, 12-48.
- Dunkin, J.W., 1965. Computation of modal solutions in layered, elastic media at high frequencies, Bull. Seism. Soc. Am., 55, 335-358.
- Evernden, J.F., 1969. Identification of earthquakes and explosions by use of teleseismic data, J. Geophys. Res., 74, 3828-3856.
- Gerver, M.L. and Kazhdan, D.A., 1968. Determination of velocity profiles from dispersion curves: problems of uniqueness, Computational Seismology 4, 78-94.
- Gilbert, F., and Backus, G.E., 1966. Propagator matrices in elastic wave and vibration problems, Geophysics, 31, 326-332.
- Hales, A.L. and Asada, T., 1966. Crustal structure in coastal Alaska, in The Earth beneath the continents, J.S. Steinhart and T.J. Smith, editors, Geophysical Monograph 10, American Geophysical Union, Washington, D.C., 420-432.

- Hamilton, W.C., 1964. Statistics in physical science, Ronald Press, New York, 230 pp.
- Hanson, K., Berg, E. and Gedney, L., 1968. A seismic refraction profile and crustal structure in central interior Alaska, Bull. Seism. Soc. Am., 58, 1657-1665.
- Harkrider, D.G., 1964. Surface waves in multilayered elastic media, I. Rayleigh and Love waves from buried sources in a multilayered elastic half-space, Bull. Seism. Soc. Am., 54, 627-679.
- Harkrider, D.G., 1968. The perturbation of Love wave spectra, Bull. Seism. Soc. Am., 58, 861-880.
- Haskell, N.A., 1953. The dispersion of surface waves on multilayered media, Bull. Seism. Soc. Am., 43, 17-34.
- HelMBERGER, D.V., 1968. The crust-mantle transition in the Bering Sea, Bull. Seism. Soc. Am., 58, 179-214.
- Herrin, E. and Goforth, T., 1977. Phase-matched filters: Application to the study of Rayleigh waves, Bull. Seism. Soc. Am., 67, 1259-1275.
- Jackson, D.D., 1972. Interpretation of inaccurate, insufficient and inconsistent data, Geophys. J., 28, 97-109.
- Jeffreys, H., 1961. Small corrections in the theory of surface waves, Geophys. J., 6, 115-117.
- Knopoff, L., 1972. Observation and inversion of surface-wave dispersion, Tectonophysics, 13, 497-519.
- McEvilly, T.V., 1964. Central U.S. crust-upper mantle structure from Love and Rayleigh wave phase velocity inversion, Bull. Seism. Soc. Am., 54, 1997-2015.

- North, R.G. and Dziewonski, A.M., 1976. A note on Rayleigh-wave flattening corrections, Bull. Seism. Soc. Am., 66, 1873-1879.
- Novotny, O., 1970. Partial derivatives of dispersion curves of Love waves in a layered medium, Studia Geophys. Geodaet., 14, 36-50.
- Oliver, J., 1962. A summary of observed seismic surface wave dispersion, Bull. Seism. Soc. Am., 52, 81-86.
- Parker, R.L., 1970. The inverse problem of electrical conductivity in the mantle, Geophys. J., 22, 121-138.
- Pedersen, L.B., 1977. Interpretation of potential field data, a generalized inverse approach, Geophys. Prosp., 25, 199-230.
- Filant, W.L. and Knopoff, L., 1970. Inversion of phase and group slowness dispersion, J. Geophys. Res., 75, 2135-2136.
- Rodi, W.L., Glover, P., Li, T.M.C., and Alexander, S.S., 1975. A fast, accurate method for computing group-velocity partial derivatives for Rayleigh and Love waves, Bull. Seism. Soc. Am., 65, 1105-1114.
- Shor, G.G., 1964. Structure of the Bering Sea and the Aleutian Ridge, Marine Geol., 1, 213-219.
- Smith, M.L. and Franklin, J.N., 1969. Geophysical application of generalized inverse theory, J. Geophys. Res., 74, 2783-2785.
- Stacey, F.D., 1977. Physics of the Earth, 2nd edition, John Wiley & Sons, New York, 414 pp.

- Takeuchi, H., Dorman, J. and Saito, M., 1964. Partial derivatives of surface wave phase velocity with respect to parameter changes within the earth, J. Geophys. Res., 69, 3429-3441.
- Thomson, W.T., 1950. Transmission of elastic waves through a stratified solid medium, J. Appl. Phys., 21, 89-93.
- Thrower, E.N., 1965. The computation of the dispersion of elastic waves in layered media, J. Sound Vib., 2, 210-226.
- Ward, S.H., Peeples, W.J. and Ryu, J., 1973. Analysis of geoelectromagnetic data, in Methods in computational physics, B.A. Bolt, editor, 13, 163-238.
- Wiggins, R.A., 1972. The general linear inverse problem: Implication of surface waves and free oscillations for earth structure, Rev. Geophys. Space Phys., 10, 251-285.
- Woollard, G.P., Ostenso, N.A., Thiel, E. and Bonini, W.E., 1960. Gravity anomalies, crustal structure, and geology in Alaska, J. Geophys. Res., 65, 1021-1037.
- Yu, G.K. and Mitchell, B.J., 1979. Regionalized shear velocity models of the Pacific upper mantle from observed Love and Rayleigh wave dispersion, Geophys. J., 57, 311-341.